Research Square

Preprints are preliminary reports that have not undergone peer review.
They should not be considered conclusive, used to inform clinical practice,
or referenced by the media as validated information.

Widespread clay–carbonate co-occurrence reveals advanced aqueous alteration on Mars

Jeremy Brossier

jeremy.brossier@inaf.it

National Institute for Astrophysics (INAF) https://orcid.org/0000-0001-7423-2494

Maria Cristina De Sanctis

National Institute for Astrophysics https://orcid.org/0000-0002-3463-4437

Francesca Altieri

National Institute for Astrophysics (INAF)

Marco Ferrari

National Institute for Astrophysics https://orcid.org/0000-0002-7447-6146

Andrea Raponi

Institute for Space Astrophysics and Planetology https://orcid.org/0000-0003-4996-0099

Vito Saggese

National Institute for Astrophysics (INAF) https://orcid.org/0009-0000-9738-0641

Monica Rasmussen

National Institute for Astrophysics (INAF) https://orcid.org/0000-0002-2816-0554

Alessandro Frigeri

Italian National Institute for Astrophysics (INAF) https://orcid.org/0000-0002-9140-3977

Simone De Angelis

National Institute for Astrophysics (INAF)

Enrico Bruschini

National Institute for Astrophysics (INAF)

Physical Sciences - Article

Keywords: Mars, Carbonates, CRISM, Survey, Aqueous Alteration

Posted Date: July 2nd, 2026

DOI: https://doi.org/10.21203/rs.3.rs-9957915/v1

License: This work is licensed under a Creative Commons Attribution 4.0 International License.
Read Full License

Additional Declarations: The authors declare no competing interests.

Widespread clay–carbonate co-occurrence reveals advanced aqueous alteration on Mars

Jeremy Brossier*, Maria Cristina De Sanctis, Francesca Altieri, Marco Ferrari, Andrea Raponi, Vito Saggese, Monica Rasmussen, Alessandro Frigeri, Simone De Angelis, Enrico Bruschini

Affiliation: Institute for Space Astrophysics and Planetology (IAPS), National Institute of Astrophysics (INAF), Rome, Italy

*Corresponding author: Jeremy Brossier (jeremy.brossier@inaf.it, brossier.jrmy@gmail.com)

ORCID: 0000-0001-7423-2494

Abstract (150 words)

Carbonates on Mars provide key evidence of past environmental conditions because they can form through alteration of ultramafic rocks by liquid water in a dense CO_2–rich atmosphere. We searched for carbonates by examining the 2.3, 2.5, and 3.5 μm absorption bands in 540 CRISM near-infrared hyperspectral cubes. The detected carbonates are best described as Fe–Mg solid solutions within the siderite–magnesite series, likely formed under reducing conditions and preserved despite later acidic, oxidizing environments. We identify new carbonate-rich deposits associated with clay-bearing terrains, revealing a more widespread co-occurrence of carbonates and clays than previously recognized, partly because carbonates can be spectrally masked by clays. Their association suggests formation in neutral to mildly alkaline waters early in Mars' history, implying prolonged aqueous alteration, sustained liquid water, and environments potentially favorable for microbial life. These findings expand the known distribution of carbonates and highlight promising targets for future biosignature exploration.

Keywords: *Mars, Carbonates, CRISM, Survey, Aqueous Alteration*

INTRODUCTION

Clays – particularly ferromagnesian (Fe,Mg-rich) smectites – are the most abundant hydrated minerals detected on Mars from orbit (1,2), while carbonates remain relatively elusive in orbital observations. Both mineral phases are important indicators of past habitability, as they typically form in neutral to alkaline aqueous environments that could sustain stable bodies of water. Since liquid water is essential for the emergence and development of life, the presence of these minerals points to ancient aqueous environments that may once have harbored life. Carbonates are especially significant because their formation implies a thicker, CO_2-rich early atmosphere capable of supporting such conditions. Although carbonates were expected to be widespread on early Mars, they are only sparsely observed from orbit, making each detection particularly valuable for reconstructing the planet's atmospheric, climatic, and hydrological history. Carbonate minerals consist of the carbonate ion (CO_3^{2-}) combined with metal cations such as Fe^{2+}, Mg^{2+} or Ca^{2+}, forming simple phases like siderite [$FeCO_3$], magnesite [$MgCO_3$], and calcite [$CaCO_3$], or more complex phases such as dolomite [$CaMg(CO_3)_2$]. Their chemical compositions and associations with other minerals can reveal their formation pathways, which generally involve interactions between liquid water and carbon dioxide, supporting the idea that Mars once experienced warmer, wetter, and more CO_2-rich conditions than today. On Mars, carbonates are commonly thought to form primarily through the aqueous alteration of olivine-rich basaltic rocks of mafic to ultramafic composition, involving surface water, shallow subsurface groundwater, and possibly hydrothermal systems at greater depths (3,4).

Carbonates on Mars were first conclusively identified from orbital spectroscopy in the Nili Fossae region and Jezero crater (3,4), with later studies reporting additional, smaller exposures elsewhere on the planet (5-7). Subsequent in situ analyses by rover missions have confirmed their presence at Gusev, Jezero, and Gale craters (8-10). Additional evidence includes small amounts of carbonates in soils surrounding the Phoenix lander (11), and a possible global dust component inferred from the Thermal Emission Spectrometer (TES) observations (12). Moreover, carbonates are identified in Martian meteorites such as Allan Hills (ALH) 84001, where they form Fe-, Mg- and Ca-rich nodules, and in others – including Lafayette, Nakhla and Governador Valadares – where they are commonly associated with clay minerals (13-15).

Despite these discoveries, carbonate-rich deposits identified on Mars remain far less abundant than expected for a planet that once had a dense CO_2 atmosphere (16,17). This scarcity suggests either that the early atmosphere contained less CO_2 than previously thought, or that carbonates have since been buried, altered, or otherwise obscured. Additionally, during the Hesperian era (roughly 3.7 to 3.0 billion years ago), widespread volcanism may have created acidic conditions that dissolved pre-existing carbonates or inhibited their formation (18,19).

Spectral identification of carbonates is particularly challenging when they are mixed with other minerals, especially in observations limited to wavelengths shorter than 2.5 µm. In this spectral range, carbonates typically exhibit absorption bands near 2.3 and 2.5 µm, which overlap with diagnostic features of other mineral phases, notably clays. Previous studies have shown that clay minerals can suppress or mask the

spectral signatures of carbonates (20) and some sulfates (21,22) over the 1–2.6 µm range. This issue is particularly relevant on Mars, where carbonates are often intimately associated with clays, especially in regions such as Nili Fossae, Jezero Crater, and others (3,7,23-25). Additionally, carbonates are sometimes detected alongside partially altered olivine, which is interpreted as precursor material (26,27).

Consequently, detecting carbonates from orbit on Mars remains challenging and requires detailed spectral analysis. Identifying these cryptic carbonate deposits would greatly enhance the astrobiological importance of such regions, as carbonates may have persisted through the mildly acidic and saline conditions of the Hesperian era and could preserve important records of past CO_2-water interactions.

In this study, we search for carbonates associated with clays, which are the most widespread alteration products on Mars (1,2) and are widely regarded as key indicators of past habitability. By reassessing the relationship between clays and carbonates, we may significantly expand the currently recognized distribution of carbonates across the planet.

RESULTS

We examine the possible co-occurrence of carbonates and clays using near-infrared hyperspectral data (1–4 µm) acquired by the Compact Reconnaissance Imaging Spectrometer for Mars (CRISM) aboard the Mars Reconnaissance Orbiter (MRO). Representative spectra from our dataset are presented in **Figure 1** alongside candidate analogue spectra from reference spectral libraries. Small amounts of carbonates are difficult to detect in remote sensing spectral observations, particularly when they are mixed with other minerals such as clays and sulfates. Carbonates are usually identified by paired absorptions at 2.3 and 2.5 µm within the 1–3 µm spectral range (**Figure 1**), as well as by deep absorptions around 3.4–3.5 µm and near 3.9 µm, which are associated with x-CO_3^{2-} vibrational modes (28). In clay-carbonate mixtures, however, the 2.3 µm absorption feature is largely controlled by the clay component, which also exhibits a clear band in this region (20,29-30). Therefore, the presence of a 2.3 µm absorption band alone is not diagnostic of carbonates, as this feature is also characteristic of ferromagnesian clays. When sulfates are present, this band can be substantially reduced or may even disappear (31), as observed at Gale crater, where Curiosity identified siderite together with sulfates (e.g., anhydrite, gypsum, kieserite) despite the absence of detectable carbonate signatures in orbital observations (10). In contrast, the 2.5 µm carbonate absorption feature is less affected by clays and sulfates, making it a more direct indicator of carbonates (**Figure 1**). However, detecting the 2.5 µm band in CRISM observations remains difficult because it is generally weak and may fall below the instrument's detection threshold. This band can also be obscured by spectral mixing (the combination of signals from multiple minerals within a single pixel) and overlapping absorption features, particularly the strong H_2O band near 3 µm, whose short-wavelength shoulder may partially mask the 2.5 µm feature. Its detectability is further reduced by spectrally neutral contributions from dust or rock coatings, which can attenuate or suppress diagnostic absorptions (32). As a result, this feature has mainly been identified from orbit in regions with relatively high carbonate abundances, such as Nili Fossae and Jezero crater, where higher concentrations help mitigate these masking effects.

Considering that the 2.3 µm absorption may indicate the presence of either clays or carbonates, we performed a detailed analysis of 540 CRISM cubes exhibiting this band. These data were drawn from a broader survey of over 1500 observations (2), mainly spanning the Martian crustal dichotomy and southern highlands. Due to instrumental limitations and intrinsic characteristics of Mars – particularly atmospheric absorptions, hydration features, and pervasive surface dust cover – the 1–2.6 µm spectral range provides the most reliable window for robust analysis. We therefore initiated our study by computing key spectral parameters within this range (see **Data & Methods**).

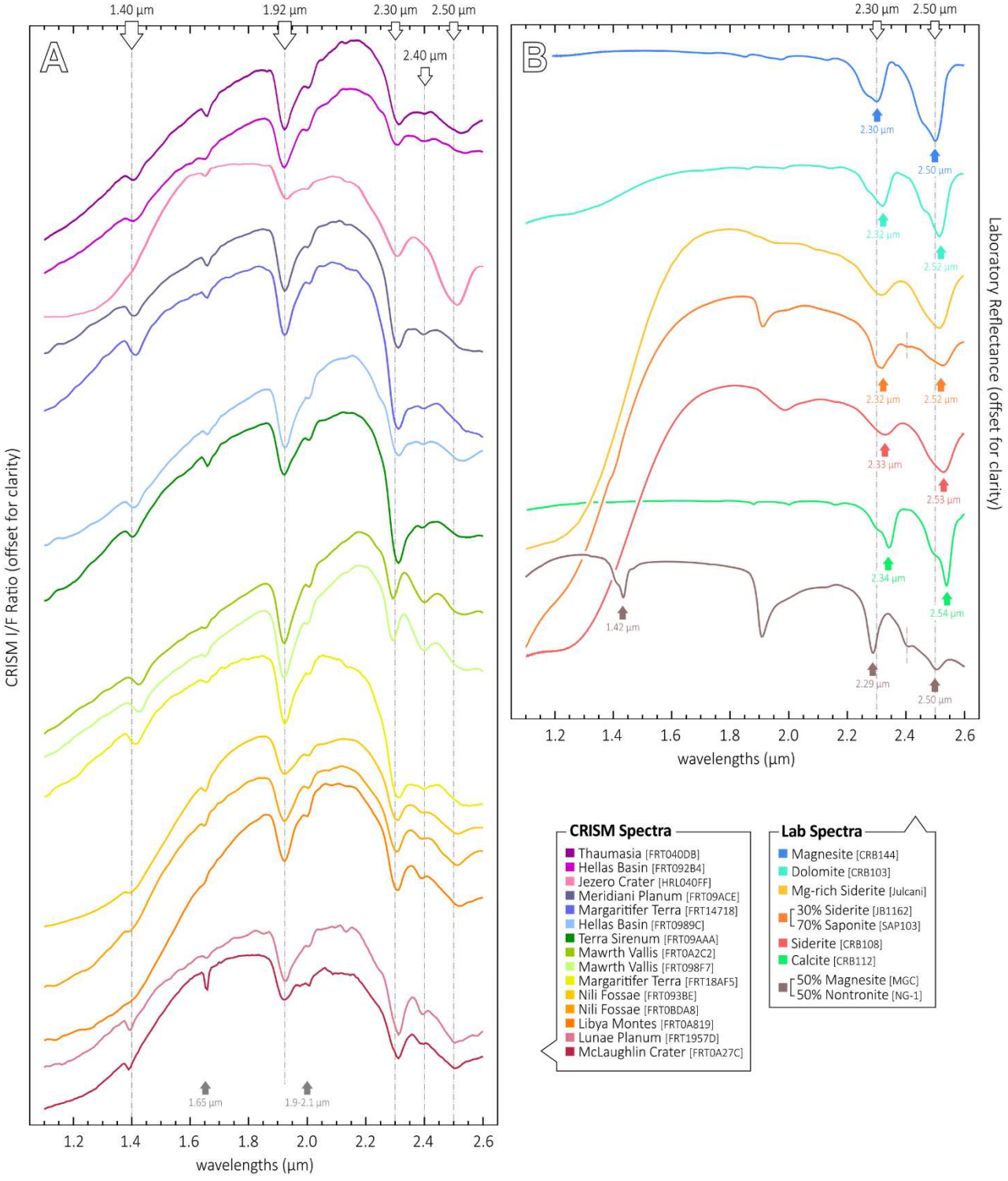


Figure 1 – (A) Representative spectra of denoised CRISM reflectance (normalized and vertically offset for clarity) for clay-bearing deposits with carbonate signatures over the 1.1–2.6 µm range. All cubes present clear absorptions at 1.4, 1.9, 2.3, and 2.4 µm, characteristic of ferromagnesian clays. Several cubes also display a recurrent absorption near 2.5 µm, suggestive of carbonates. Data are considered unreliable at (1) 1.65 µm due to intermittent spikes from a detector filter boundary, (2) 1.9–2.1 µm owing to residual noise from atmospheric removal pipeline (33,34), and (3) 2.7–2.8 µm affected by saturated atmospheric CO_2 absorption (35). (B) Laboratory reference spectra for candidate carbonates (magnesite, siderite, calcite, and dolomite) from the RELAB database and SSHADE repository. Examples include Fe-rich saponite associated with Mg-rich siderite (dark orange), and nontronite mixed with magnesite (brown). Pure carbonates display characteristic paired absorptions near 2.3 and 2.5 µm, whereas mixtures with clays produce additional bands at 1.4, 1.9, and 2.4 µm. Fe–Mg carbonates (orange) may also display absorption bands comparable to those of dolomite (cyan).

Regarding the 2.3 µm absorption, our dataset shows band positions ranging from 2.29 to 2.32 µm, consistent with ferromagnesian compositions (**Figure 1**). More specifically, for clay-dominated assemblages, an absorption at 2.29 µm indicates Fe-rich clays (nontronites), while an absorption at 2.32 µm is characteristic of Mg-rich clays (saponites) (2,36). Band centers at intermediate wavelengths may indicate the presence of vermiculite, ferrosaponite, or alternatively reflect mixtures of multiple components. Overall, the average 2.3 µm band center is located at 2.302 ± 0.007 µm (standard deviation, 1σ) (**Figure 2A**), consistent with both the clay minerals and some carbonates. Strongest absorptions, centered near 2.305-2.311 µm, are mainly observed in Nili Fossae and Jezero crater (dark red; **Figure 2**), consistent with earlier studies (3,4) in which carbonates were identified unambiguously. All band centers and depths extracted in this work are reported in the Supporting Information (BC23 and BD23; **Table S1**).

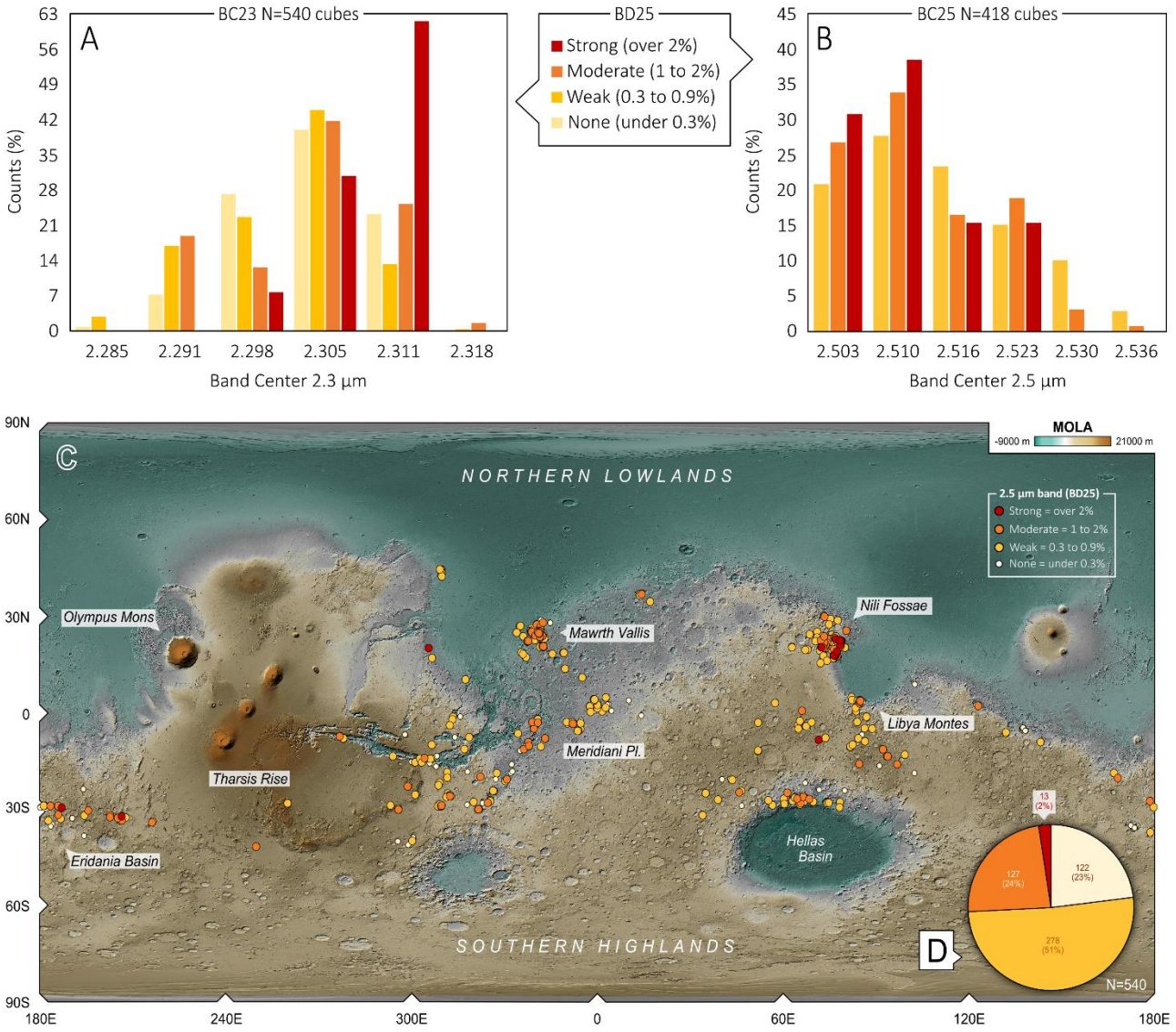


Figure 2 – (A,B) Band centers for the 2.3 and 2.5 µm absorptions were determined after continuum removal to enhance band contrast. Values are subdivided according to the intensity of the 2.5 µm band observed in this survey, expressed as band depth values (BD25; ***Table S1****): none (below 0.3%), weak (0.3-0.9%), moderate (1-2%), and strong (above 2%). For the 2.3 µm absorption, band centers range from 2.29 to 2.32 µm (A), whereas for the 2.5 µm band they span 2.50 to 2.54 µm (B). The mean values are 2.302 ± 0.007 µm and 2.514 ± 0.009 µm, respectively. (C) Global map of Mars showing colorized MOLA topography and the distribution of clay-bearing outcrops with associated carbonates, based on a survey of 540 CRISM targeted cubes. Band depth at 2.5 µm shows substantial variability, ranging from low values of 0.3–0.9% (yellow) to moderate values of 1–2% (orange), and exceeding 2% in the strongest cases (red). All measurements of the 2.3 and 2.5 µm absorption bands are reported in* ***Table S1****. For approximately 122 spectra, the 2.5 µm band center could not be determined due to limited data quality or because the absorption was too weak or simply absent. See also* ***Figure S1.1*** *(Supporting Information) for a detailed comparison of the relative strengths of the 2.3 and 2.5 µm bands. (D) Pie chart showing the relative frequencies of clays and possible carbonates identified in this study; paired absorptions at 2.3 and 2.5 µm are clearly detected in 418 cubes. Numbers labeled in each segment indicate the corresponding detection counts.*

The 2.5 µm absorption band remains an important spectral feature for identifying and characterizing carbonates. Because this band is often extremely weak, it is difficult to detect using standard spectral index maps (37,38). For this reason, we employed an ad hoc approach, as detailed in the **Data & Methods**. In this study, we investigated its presence across 540 selected cubes already showing the 2.3 µm band and detected a measurable 2.5 µm band in 418 of them (approximately 77%), albeit with highly variable intensity (**Figure 2**). Measured band depths generally range from relatively subtle values of about 0.3–0.6% at Oxia Planum (24,25) and Xanthe Terra (39) to substantially stronger absorptions in Nili Fossae and Jezero crater – regions where carbonates have previously been identified (3,4) – reaching up to 3% in our estimates. Band centers and depths derived for each cube are reported in the Supporting Information (BC25 and BD25; **Table S1**).

Band centers range from 2.50 to 2.54 µm, with a mean value of 2.514 ± 0.009 µm (**Figure 2B**). Most values are concentrated near 2.51 µm, with only a few outcrops showing weaker absorptions above 2.53 µm and none observed below 2.50 µm. The exact positions of carbonate absorptions in the 2.3–2.5 µm region are strongly influenced by their composition, particularly the mass of the major cation (such as Mg, Fe, or Ca) in the mineral structure. Lighter cations like Mg^{2+} result in absorptions at shorter wavelengths (e.g., 2.50 µm for Mg-rich carbonates like magnesite), while heavier cations like Fe^{2+} or Ca^{2+} shift the absorption to longer wavelengths (e.g., siderites and calcites) (28,40). Additional details on relevant carbonate analogues are provided in ref. (28) and in the supporting information (**Table S2**).

To further support our analysis, we extended our investigation to spectral signatures beyond 3 µm (7,23). Interpretation of this spectral region (3–4 µm) in the CRISM data can be deceptively difficult due to several factors: (1) the lack of correction for the thermal emission, which weakens absorption band depths (41,42); (2) the significantly lower detector signal-to-noise ratio – roughly four times lower than in the 1–3 µm range; and (3) the presence of a deep water absorption around 3 µm alongside an instrumental artifact near 3.2 µm that may obscure the carbonate-related features (43).

Despite these limitations, analyzing multiple spectral features allows for a more robust and reliable identification and characterization of carbonates on Mars. Carbonates typically exhibit deep absorptions near 3.4–3.5 µm and around 3.9 µm (**Figure 3**). Variations in the position of the 3.4–3.5 µm band provide information about carbonate composition, with magnesite showing absorptions near 3.42 µm and siderite or calcite near 3.45–3.50 µm (23,28) (**Table S1**). However, as noted in ref. (3) and subsequent studies, this diagnostic band is often weak or absent in Martian data, most likely because the strong water absorption feature near 3 µm partially obscures or overlaps with the carbonate signal.

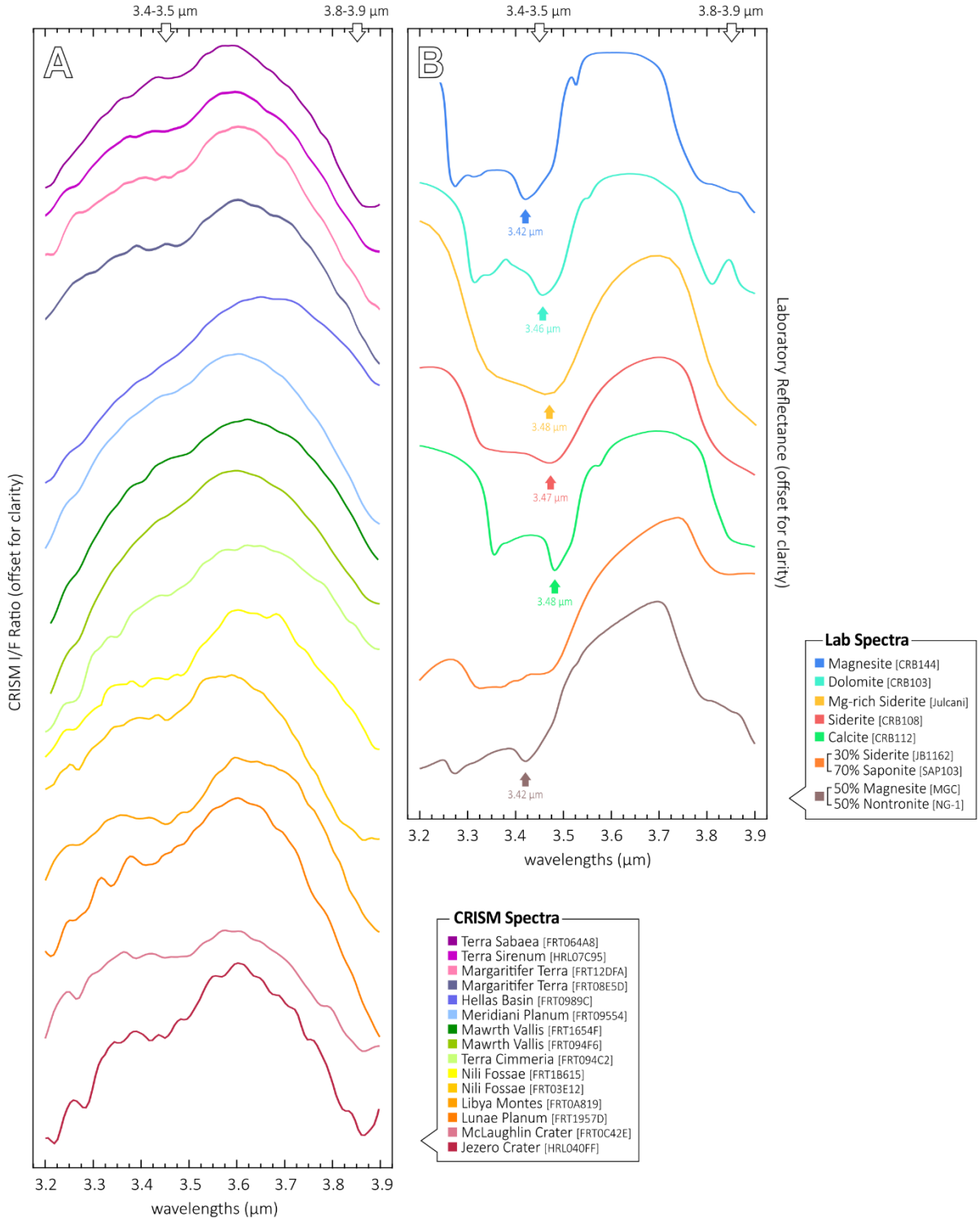


Figure 3 – (A) Representative spectra of denoised CRISM reflectance (normalized and vertically offset for clarity) for clay deposits with possible carbonates in the 3.2–3.9 µm range. All spectra exhibit a broad "bulge-like" feature near 3.6–3.7 µm, characteristic of carbonates on Mars (3,7,23). Unusable data near 3.2 µm is due to an instrumental artifact, and at 3.9 µm related to filter boundary (35,43). (B) Laboratory spectra of typical candidate carbonates (magnesite, siderite, calcite, and dolomite) and mixtures with clays extracted from the PDS Geosciences Node Spectral Library bundle containing the RELAB database.

Nevertheless, by analyzing the 418 cubes showing the 2.5 µm feature, we identify possible absorption band centers between 3.44 and 3.50 µm in 342 cubes, yielding an average value of 3.481 ± 0.020 µm (**Figure 4A**), consistent with previous findings (7,23). Moreover, carbonates exhibit a broad composite feature centered between 3.4 and 3.9 µm (**Figure 3**), typically resulting from the combination of diagnostic carbonate absorptions (28). This spectral signature, also referred to as the "bulge-like" feature, has been identified in carbonates on Mars (3,7,23). Conversely, many other minerals commonly found on Mars display a steadily increasing reflectance within the 3.4–3.9 µm range without discernible absorptions (44,45).

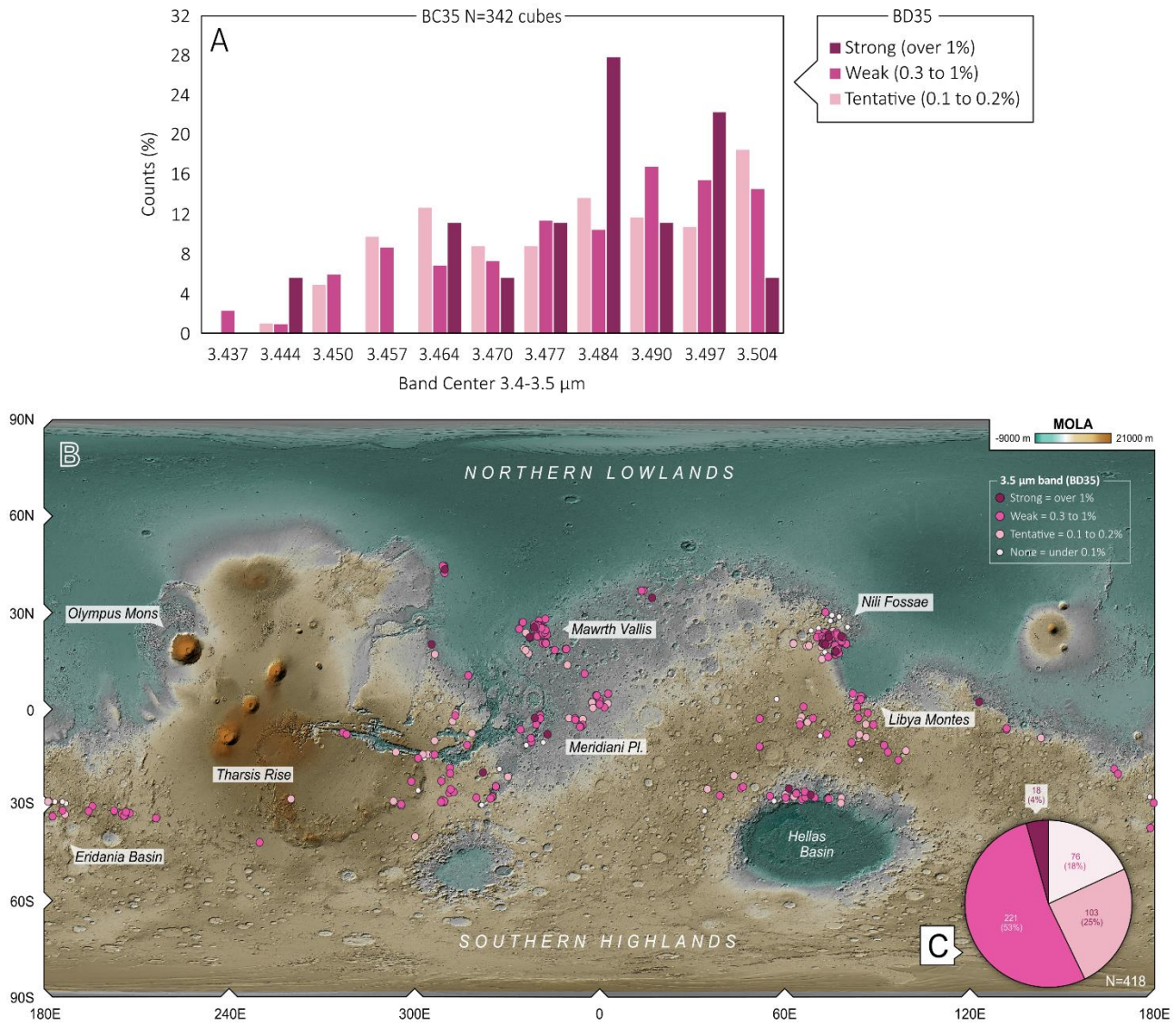


*Figure 4 – (A) Band centers for the 3.5 µm absorption were determined, where present, after continuum removal to enhance band contrast and improve readability. Values are subdivided according to the intensity of the 3.5 µm band, expressed as band depth values (BD35; **Table S1**): tentative detection (0.1–0.2%), weak (0.3–1%), and strong (above 1%). In this window, values range from 3.44 to 3.50 µm, with a mean value of 3.481 ± 0.020 µm. (B) Global map of Mars showing colorized MOLA topography and the distribution of selected cubes showing paired absorptions at 2.3 and 2.5 µm. A subset of these cubes also displays a weak absorption near 3.5 µm and a reflectance drop around 3.9 µm, both characteristic of carbonates on Mars. Clear detections are shown in light purple (weak: 0.3–1%) and dark purple (strong: over 1%), whereas*

tentative detections (0.1–0.2%) are indicated in pink. (C) Pie chart illustrating the relative frequencies of absorptions identified in this study; all three bands (2.3, 2.5, and 3.5 µm) are collectively detected in 342 cubes.

Although the 3.8–3.9 µm absorption cannot be entirely resolved due to the limited CRISM spectral range, it can still be retrieved from a sudden reflectance drop near 3.9 µm. Most of the areas analyzed here show the expected carbonate-related features within the 3–4 µm range (**Figure 3**). Following the approach already used in literature (3,23,25), we computed the band depth near 3.9 µm ("*BD3900*") to assess carbonate presence and distribution across the selected outcrops (see **Figures S2.1 and S2.2** in Supporting Information).

Figure 4 illustrates the spatial distribution of CRISM targeted cubes in which we identified carbonate-related spectral absorptions. All three diagnostic bands (2.3, 2.5, and 3.5 µm) are jointly observed in 342 cubes, with different levels or robustness. More specifically, the 3.5 µm absorption is clearly resolved in 239 cubes, from relatively low values (0.3–1%) to high values (over 1%). Conversely, it is only marginally discernible in 103 cubes, with band depths close to the noise level (**Figure S1.2**). As for the 2.3 and 2.5 µm absorption bands, the band centers and depths measured for the 3.5 µm absorption are provided in the Supporting Information (BC35 and BD35; **Table S1**). The remaining 76 cubes show no clearly detectable absorption near 3.5 µm, most likely due to incomplete spectral coverage or reduced data quality in this spectral region.

Detailed analysis on this large dataset reveals the co-occurrence of multiple absorption bands at 2.3, 2.5, 3.5, and 3.9 µm, consistent with the presence of carbonates in most of the examined cubes. In the majority of cases where the 2.3 µm band is detected, a corresponding 2.5 µm absorption is also present. The 3.5 µm band is more difficult to isolate in our dataset for the reasons outlined above. Accordingly, the classification hierarchy reflects both the relative strength of these bands and their detectability. More than 500 occurrences of the 2.3 µm band are identified, over 400 of which also exhibit the 2.5 µm band, while more than 300 show the combined presence of the 2.3, 2.5, and 3.5 µm bands.

Where carbonates and clays co-occur, intensities of their absorption features are expected to covary, as carbonates contribute to the 2.3 µm band. Accordingly, even in mixtures with variable proportions, an increase in carbonate content should generally produce a deeper 2.3 µm absorption (see **Data & Methods**). The scatterplot of 2.3 versus 2.5 µm band depths for the 418 cubes (**Figure 5**) reveals a positive but scattered correlation between the two parameters. A zero-intercept fit yields $R^2 = 0.83$ ($p << 0.001$), consistent with the expectation that zero band depth corresponds to the absence of detectable absorption features, although the low band depth regime is affected by detection thresholds of around 0.3–0.5%. Under this assumption, spectra with deeper 2.3 µm absorptions systematically exhibit stronger 2.5 µm bands, approximated by $BD_{2.5} = 0.33 \times BD_{2.3}$. Importantly, no observations exhibit a strong 2.3 µm absorption without an accompanying 2.5 µm feature, suggesting the absence of spectrally pure, abundant clays within this dataset. This behavior is consistent with spectral mixing effects (see **Data & Methods**). Thus, the apparent progressive decrease in

identifications primarily reflects the increasing difficulty to detect these features; they are likely present in many additional cubes but fall below the detection threshold.

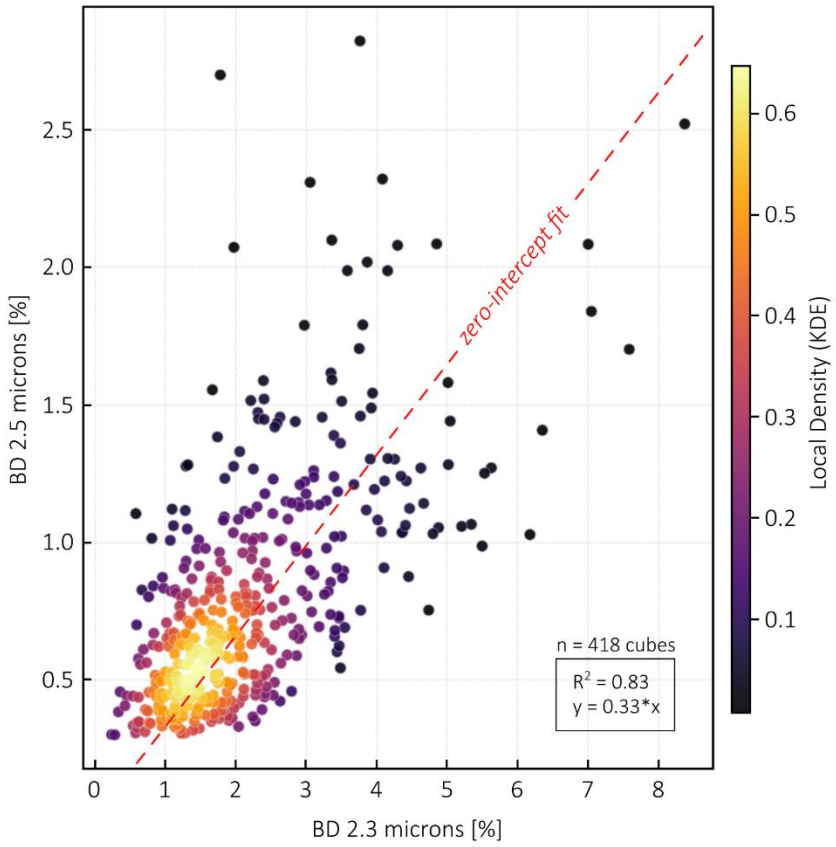


Figure 5 – Scatterplot of the 2.3 versus 2.5 µm band depths for the 418 selected CRISM cubes showing both absorption features. Each point represents a mean spectrum and is colored according to local point density (KDE). The dashed red line represents the zero-intercept linear fit BD25 = 0.33×BD23 with R^2=0.83. The positive correlation between the two band depths supports the presence of carbonates together with clays.

Some terrestrial phyllosilicate species, such as serpentines and chlorites, also display absorption bands near both 2.3 and 2.5 µm, which can potentially mimic carbonate signatures. Mg-rich serpentines (e.g., lizardite, antigorite, and chrysotile) typically show absorptions near 1.38, 2.12, 2.33, and 2.52 µm (46). The 2.12 µm band is generally weak, while the 2.5 µm band varies in width and depth depending on the serpentine species (46,47). Chlorites (e.g., clinochlore) display a strong absorption near 2.33–2.35 µm, along with weaker bands at 2.10–2.12 µm and around 2.47 µm (46). In Fe-rich chlorites (e.g., chamosite, thuringite), these features shift to longer wavelengths, with the 2.3 µm band near 2.36 µm and the weaker 2.5 µm band near 2.51 µm (36,47). Additionally, chlorites can be distinguished from serpentines by a sloping shoulder around 2.25–2.26 µm, which is associated with aluminum substitutions.

It is worth noting that, for both serpentines and chlorites, the absorption feature near 2.3 µm typically occurs at longer wavelengths than those observed in our dataset, in which absorption positions never exceed 2.32 µm (**Figure 1**). Instead, the absorption positions identified here are more consistent with

ferromagnesian smectites, including nontronite, saponite, and possibly vermiculite. Furthermore, serpentines or chlorites are usually associated with an additional absorption feature near 2.1 μm; however, this region may be partially obscured by systematic residual noise between 1.9 and 2.1 μm introduced during atmospheric correction (33,35). Nevertheless, the absence of a detectable 2.1 μm band in our spectra suggests that serpentines and chlorites are either absent or present only in minor abundances mixed with other phases. Although the occurrence of minor or secondary phases cannot be excluded, the dominant spectral signatures are most plausibly explained by mixtures of Fe,Mg-rich clays and carbonates.

DISCUSSION

An important implication of our results is that carbonates on Mars can be present even when the diagnostic 2.5 μm absorption falls below conventional detection thresholds. As a result, carbonate-bearing deposits may be systematically underdetected in orbital datasets. This interpretation is further supported by recent rover observations that revealed carbonate abundances of up to ~37 wt% in rocks from Jezero crater, and 5–11 wt% in materials from Gale crater, despite the absence of any detectable 2.5 μm absorption in orbital data (10,27). Collectively, these findings suggest that the currently mapped distribution of carbonates on Mars likely represents only a lower bound, and that their true abundance within the Martian crust may be significantly greater than previously estimated.

The dominant carbonate species within these assemblages cannot be unambiguously identified. CRISM data analyzed here show band centers spanning those of Fe,Mg-rich carbonates, siderites, dolomites and, to a lesser extent, calcites (**Figure 6**). However, most observed band positions overlap with siderites and Fe,Mg-rich carbonates within the siderite–magnesite solid-solution series (often called "*magnesiosiderite*" or "*ferromagnesite*"), suggesting these species as the most plausible candidates. Notably, several studies have shown that Fe-rich carbonates (siderites) generally show weaker near-infrared absorption bands than Mg-rich carbonates (magnesites), thereby limiting their detectability on Mars (4,28,48). Furthermore, siderites and magnesites are widely considered the most likely carbonate phases on Mars, as they align with the planet's geochemical, thermal, and hydrological evolution – unlike calcites or dolomites (49-51).

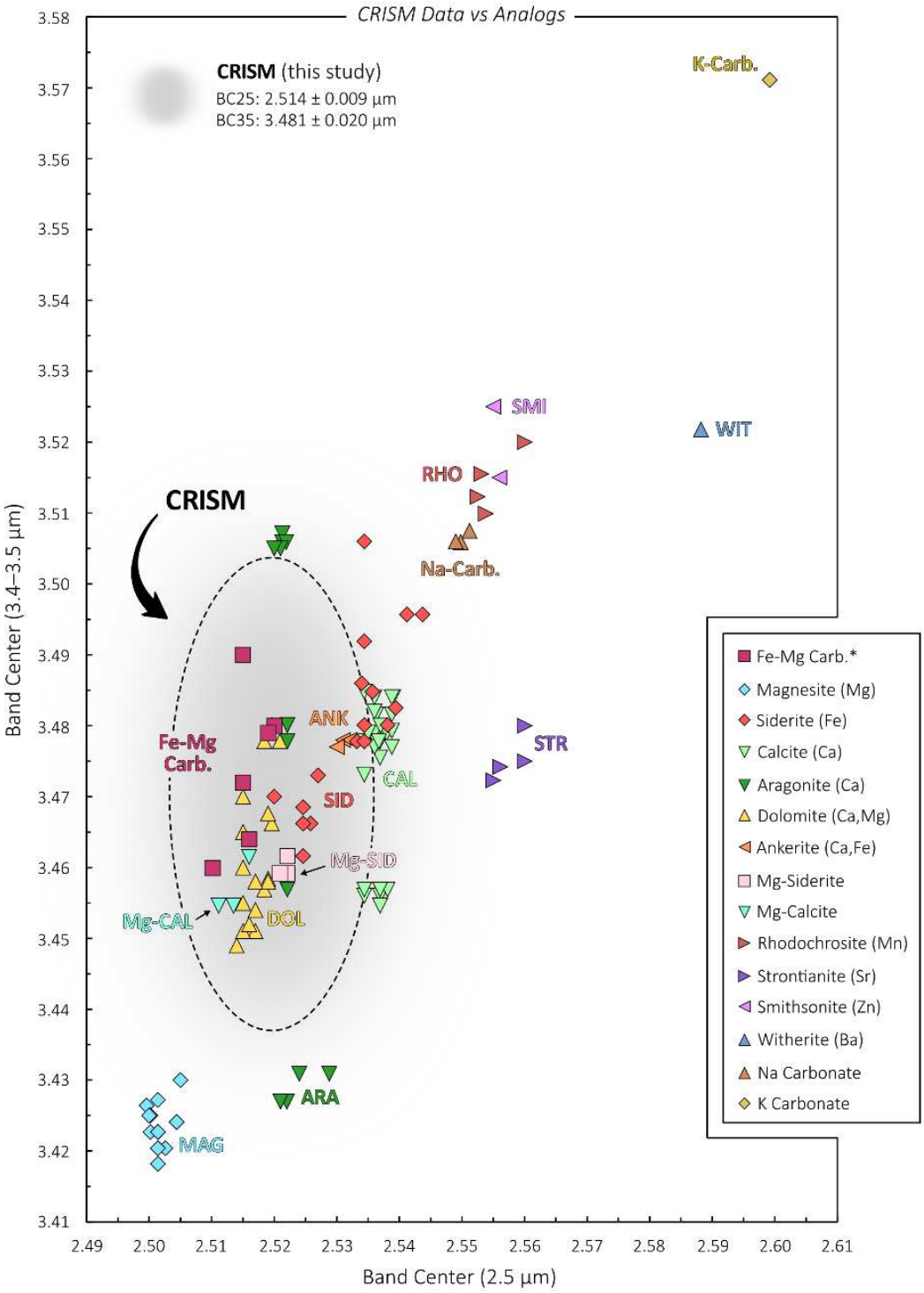


*Figure 6 – (A) Scatterplots comparing absorption band centers near 2.5 and 3.5 µm. The 342 CRISM cubes exhibiting all three diagnostic bands (2.3, 2.5, and 3.5 µm; this study) cluster within 2.50–2.54 µm and 3.44–3.50 µm (**Table S1**). These data are compared with spectra of terrestrial carbonate analogues, including siderites, dolomites, calcites, and magnesites from ref. (28), as well as selected Fe–Mg carbonates (red squares) from ref. (52). Mg-siderite samples (pink squares) are derived from ref. (53) with an average composition of $(Fe_{0.65}Mg_{0.33}Mn_{0.02})CO_3$. Most analogue spectra are stored in the RELAB database, while Fe–Mg carbonate spectra from ref. (52) are available through the SSHADE repository. Metadata for all*

*analogue samples (e.g., sample IDs, band center positions, and data sources) are given in the Supporting Information (**Table S2**).*

The detailed analysis presented here indicates that clays and carbonates co-occur more frequently than previously expected. These findings, together with the inferred kind of carbonate composition, likely Fe–Mg carbonates (magnesiosiderite, ferromagnesite) provide important constraints on the processes responsible for their formation.

Martian basalts are enriched in Fe and Mg that can supply abundant Fe^{2+} and Mg^{2+} ions through aqueous alteration in CO_2-bearing fluids, thereby favoring the precipitation of Fe–Mg carbonates. In line with this process, carbonates are often found in close spatial and genetic association with olivine-rich lithologies (27), and their compositions are therefore expected to reflect those of the olivine (54). Ref. (55) showed that carbonate-rich rocks in both Nili Fossae region and Gusev crater are dominated by Fe-Mg carbonates alongside olivine spanning a range of forsterite contents, highlighting compositional parallels between the olivine precursors and their carbonate alteration products. Martian carbonates are likely to form a continuous siderite–magnesite solid solution. Extensive Fe^{2+} and Mg^{2+} substitutions within this series are consistent with previous observations (3,8-10). For instance, carbonate-rich deposits in Jezero crater exhibit Fe–Mg phases with varying iron and magnesium contents along the traverse of Perseverance rover (9,30,56). At Gale crater, Curiosity rover has detected more sideritic signatures, ranging from nearly pure siderite to slightly Mg-enriched varieties (10,57). Additionally, analyses conducted by the Spirit rover at Gusev crater revealed Fe,Mg-rich carbonates containing only minor Ca and Mn components (8), later confirmed by CRISM observations (58). Despite differences in formation settings, these compositions closely resemble the average carbonate chemistry reported for the Martian meteorite ALH 84001 (13,59).

In contrast to Earth, where dolomite, calcite, and aragonite are the most abundant carbonates (60,61), magnesite and siderite appear to be the dominant carbonate species on Mars (3,62). Divergences in carbonate chemistry between Mars and Earth likely reflect fundamental differences in their aqueous environments (50). Dolomite formation is kinetically slow (inhibited) and requires long-lived, chemically stable aqueous systems, sufficient mobility of Mg and Ca, and moderate temperatures (63-66). Climate and hydrologic models indicate that such conditions were neither widespread nor persistent on Mars, instead occurring episodically during intermittent warm and wet intervals (67-69). Consistent with this interpretation, the carbonate record on Mars – dominated by Fe- and Mg-rich compositions – suggests that even relatively simple carbonate phases, such as magnesite, siderite, and calcite, formed only under restricted conditions, further reducing the likelihood of dolomite formation (27,50).

Similarly, calcite and its polymorph aragonite are considered unlikely candidates for Martian carbonates. In Fe- and Mg-rich environments such as those on Mars, the abundance of Fe^{2+} and Mg^{2+} ions strongly influences carbonate precipitation, inhibiting calcite formation while preferentially stabilizing magnesite and siderite. Laboratory experiments demonstrate that increasing Mg/Ca ratios markedly slow calcite growth, as Mg^{2+} effectively inhibits its precipitation (70-72). Consistent with these results, orbital and in situ rover

observations on Mars have predominantly identified siderites and magnesites, with only limited evidence of calcites (9-10,73). Our findings, based on the 2.5 vs 3.5 µm band centers (**Figure 6**), further support that siderites and magnesites are the predominant carbonate species on Mars.

The observed band positions among Fe–Mg carbonate samples (**Figure 6**) primarily reflect compositional and structural variations, as well as environmental influences (52,74-75). For instance, siderite forms an extensive solid-solution series with magnesite, and substitution of Fe^{2+} by Mg^{2+} alters the vibrational frequencies of the carbonate (CO_3^{2-}) groups due to differences in cation mass and ionic radius. Lighter cations such as Mg^{2+} produce higher frequency (shorter wavelength) absorption bands, whereas heavier cations like Fe^{2+} yield lower frequency (longer wavelength) ones. This compositional variation largely accounts for the observed band shifts seen at 2.3, 2.5, and 3.5 µm, which correspond to overtones and combination modes of CO_3^{2-} stretching and bending (28,44,76). Other minor band shifts may arise from changes in oxidation state of iron (Fe^{2+} to Fe^{3+}) during weathering or alteration processes, as seen with ferromagnesian clays (2,77).

Fe^{2+} is stable under reducing to mildly oxidizing conditions but readily oxidizes to Fe^{3+} under strongly oxidizing environments, leading to the formation of ferric oxides over time (i.e., hematite, goethite or even ferrihydrite) (78). Conversely, Mg^{2+} remains stable across both oxidizing and reducing conditions. Consequently, mixed Fe–Mg carbonates could initially precipitate while Fe^{2+} is still available and subsequently evolve toward more Mg-rich compositions through partial oxidation or Mg enrichment (50,79-80). Upon oxidation, sideritic carbonates may become progressively enriched in Mg, resulting in the preservation of deposits that appear magnesite-like in current observations (3,62). This scenario likely varied regionally on Mars, depending on local redox conditions and fluid availability, and may provide a plausible explanation for the preservation and detection of Martian carbonates. Early Fe-rich carbonates could have formed under reducing conditions and later altered or oxidized, leaving behind Mg-dominant phases observable today.

Beyond Mars, the association between clays and carbonates is fairly common across the Solar System. On Ceres, distinct carbonate phases are ubiquitous and are closely associated with pervasive clays and salts (81,82). Likewise, both clays and carbonates have been identified in samples returned from the near-Earth asteroids Ryugu and Bennu (83,84). Moreover, carbonaceous (CM) chondrites contain carbonates intimately associated with abundant clays (85-87).

On Earth, the co-occurrence of clays and carbonates is ubiquitous, reflecting a wide range of geological and geochemical environments. Such mineral associations are commonly found in sedimentary, hydrothermal, and volcanic settings. For example, in marls and lacustrine deposits (88,89) where alternating clay- and carbonate-rich layers record fluctuating aqueous and climatic conditions. They are also characteristic of hydrothermal alteration zones, where fluid-rock interactions produce secondary clays and carbonates (4,90). Additionally, they form in soils and weathering profiles, where pedogenic carbonates precipitate within clay-rich horizons under semi-arid conditions (91,92). Modern alkaline environments further demonstrate that

clays and carbonates can co-precipitate directly from aqueous solutions under evaporative and alkaline conditions (93,94). Collectively, these terrestrial examples illustrate that the simultaneous formation of clays and carbonates arises from diverse aqueous and geochemical processes involving liquid water and fluid-rock interactions – conditions that appear to have been similarly prevalent on other planetary bodies.

CONCLUSION(S)

The widespread co-occurrence of clays and carbonates revealed in this study provides new insights into the nature and extent of aqueous alteration on Mars. At the spatial resolution of CRISM, the lack of clear serpentine signatures within these assemblages suggests that alteration pathways progressed beyond early-stage serpentinization toward more evolved mineralogical systems dominated by clays and carbonates. Although the relative timing of clay and carbonate formation cannot be uniquely constrained from orbital data, the observed assemblages are consistent with either coprecipitation in neutral-to-alkaline aqueous environments or a sequential evolution, in which Fe–Mg clays formed during early stages of alteration and were subsequently followed by Fe–Mg carbonates as fluids evolved toward carbonate saturation (23,95).

Moreover, the widespread association of these minerals across multiple regions indicates advanced and spatially extensive aqueous alteration processes operating at regional to possibly global scales. This interpretation differs from previous models that emphasized olivine-carbonate associations as evidence for more localized or incomplete alteration (27,96). At smaller spatial scales or within specific geological settings, more complex and heterogeneous mineralogical associations may also occur, including mixtures involving serpentine or other minor phases. Such complexities, however, are not fully resolved at orbital resolution and will require further investigation through higher-resolution or in situ measurements.

Despite these uncertainties, the dominant signal observed in CRISM data is most consistent with advanced and mature alteration systems involving both clays and carbonates, indicating long-lived and regionally pervasive aqueous activity with important implications for the early Martian carbon cycle. On Mars, such conditions likely favored the emergence of life, as the co-occurrence of clays and carbonates is characteristic of environments considered potentially habitable and capable of preserving biosignatures over geological timescales. Their close association further implies the existence of substantial carbonate reservoirs, consistent with a CO_2-rich and sufficiently dense early atmosphere capable of sustaining stable liquid water. Collectively, these observations provide new constraints on the nature and extent of aqueous alteration on Mars, suggesting processes that may have been more advanced, persistent, and spatially widespread than previously recognized.

Data Availability Statement

CRISM targeted products are accessible through the interactive CRISM map interface (http://crism-map.jhuapl.edu/), which provides direct links for downloading each cube of interest. HiRISE imagery is similarly available via the "*HiWish*" repository maintained by the Lunar and Planetary Laboratory (https://www.uahirise.org/hiwish/browse). Otherwise, all CRISM and HiRISE datasets are archived on the

NASA Planetary Data System (PDS) server (https://ode.rsl.wustl.edu/mars/). Laboratory spectra were obtained from the PDS Geosciences Node Spectral Library, including the RELAB database (https://pds-speclib.rsl.wustl.edu/search.aspx). The full dataset and accompanying GIS-ready shapefile are publicly available through the Figshare repository (97), thereby facilitating ongoing and future research efforts.

Funding

This work is supported by the Italian Space Agency (ASI), with the project ASI-INAF n.23-3-HH.0.

Author Contributions

J.B., M.C.D.S., and F.A. conceived the study. J.B. collected, analyzed, and interpreted the data. M.C.D.S. and F.A. supervised the project. A.R. performed the spectral mixing modeling. J.B. wrote the manuscript, and all authors reviewed and revised it.

Competing Interests

The authors declare no competing interests.

Materials & Correspondence

Correspondence and requests for materials should be addressed to J.B.

DATA & METHODS

CRISM targeted data and spectral survey

Near-infrared wavelengths contain diagnostic absorptions of many key mineral phases (e.g., clays, sulfates, and carbonates), enabling their detection on the Martian surface (43,98-100). These minerals display a strong absorption near 1.9 µm, along additional diagnostic bands within the 2.2–2.6 µm spectral range, enabling their discrimination in orbital spectroscopic surveys (1,2): (1) aluminous clays (e.g., montmorillonites, kaolinites) and hydrated silica (e.g., opalines) display absorptions near 2.21 µm, (2) ferromagnesian clays (e.g., nontronites, saponites) exhibit absorptions at 2.29–2.32 µm, (3) chlorites and prehnites are characterized by absorptions near 2.35 µm, (4) mono- and polyhydrated sulfates show combined absorptions near 1.9 or 2.1 µm and 2.4 µm, and (5) carbonates are identified by paired absorptions near 2.3 and 2.5 µm. Moreover, the near-infrared range is less affected by ferric minerals (iron oxides) in rock coatings and surficial dust than visible wavelengths (101,102). Spectral signatures of clay-bearing deposits were obtained from infrared observations gathered by the CRISM instrument covering the 1–4 µm range (35,43). The instrument provides a spatial resolution of approximately 18–36 $m \cdot px^{-1}$ and a spectral sampling of 6.6 nm in its so-called "*targeted*" mode. Among over 1500 CRISM targeted observations analyzed in our previous survey (Brossier et al. 2026), we selected 540 cubes showing clear signatures of ferromagnesian clays, including 471 Full-Resolution Targeted (FRT), 53 Half-Resolution Long (HRL), and 16 Half-Resolution Short (HRS) cubes.

Some regions, particularly Mawrth Vallis, Nili Fossae and Meridiani Planum, were strongly prioritized during the nominal phase of the Mars Reconnaissance Orbiter mission (43), resulting in a disproportionately large number of targeted observations by the CRISM instrument in these areas. In our dataset, Mawrth Vallis, Nili Fossae, and Meridiani Planum contribute 71, 106, and 47 cubes, respectively – together accounting for 40% of all analyzed cubes in this survey. To evaluate whether this uneven sampling affects the global interpretation, we present additional histograms and pie charts that exclude these heavily sampled regions (**Figure S3**). Nevertheless, the relative distributions of the observed absorption bands near 2.5 and 3.5 µm and their exact positions remain largely unchanged.

All selected cubes were collected during the nominal phase of the MRO mission, when CRISM performance was optimal (2006–2012). Later observations were excluded due to increased detector noise following the cryocooler failure, which raised detector temperature and degraded data quality over time (103-105). Key metadata of all 540 analyzed cubes including labels, coordinates, acquisition dates, and targeted regions are given in **Table S1** (see Supporting Information).

CRISM targeted cubes were first downloaded from the Planetary Data System (PDS) server and processed using ENVI Classic (v.5.4) with the CRISM Analysis Toolkit (CAT, v.7.4) to apply standard atmospheric and photometric corrections (106). Corrected cubes were subsequently denoised using a "*column-by-column*" ratioing approach, in which each pixel spectrum was divided by the median spectrum of its column (2,25). The median spectrum, being spectrally bland (featureless), serves as a baseline to greatly reduce detector

noise (column-dependent) and most residual atmospheric absorptions, thereby enhancing diagnostic mineral absorptions (2,25,104).

After correction and denoising, band depths at 1.9 and 2.3 µm were calculated to identify pixels showing the strong paired absorptions characteristic of ferromagnesian clays on Mars (1,2), thereby delineating the regions of interest (ROIs). For each cube, band depths were derived using the standard "*BD1900R2*" and "*D2300*" parameters defined by ref. (38). Initial detection thresholds require band depths exceeding 1% at 1.9 µm and 0.5% at 2.3 µm, with small adjustments depending on data quality and noise levels (2,25). These thresholds were then refined on a cube-by-cube basis by determining the minimum values needed to clearly distinguish the targeted outcrops from background noise. Their robustness can also be assessed by cross-referencing with higher-resolution imagery, in which the corresponding outcrops generally exhibit distinctive morphologies and tonal contrasts relative to surrounding areas (**Figure 7**). For instance, clay-bearing outcrops at Oxia Planum commonly appear layered, light-toned, and fractured in images acquired by the High-Resolution Imaging Science Experiment (HiRISE) (24,25). Additional details on the procedure used to identify clay-bearing deposits and their distribution (ROIs) are provided in our previous studies (2,25).

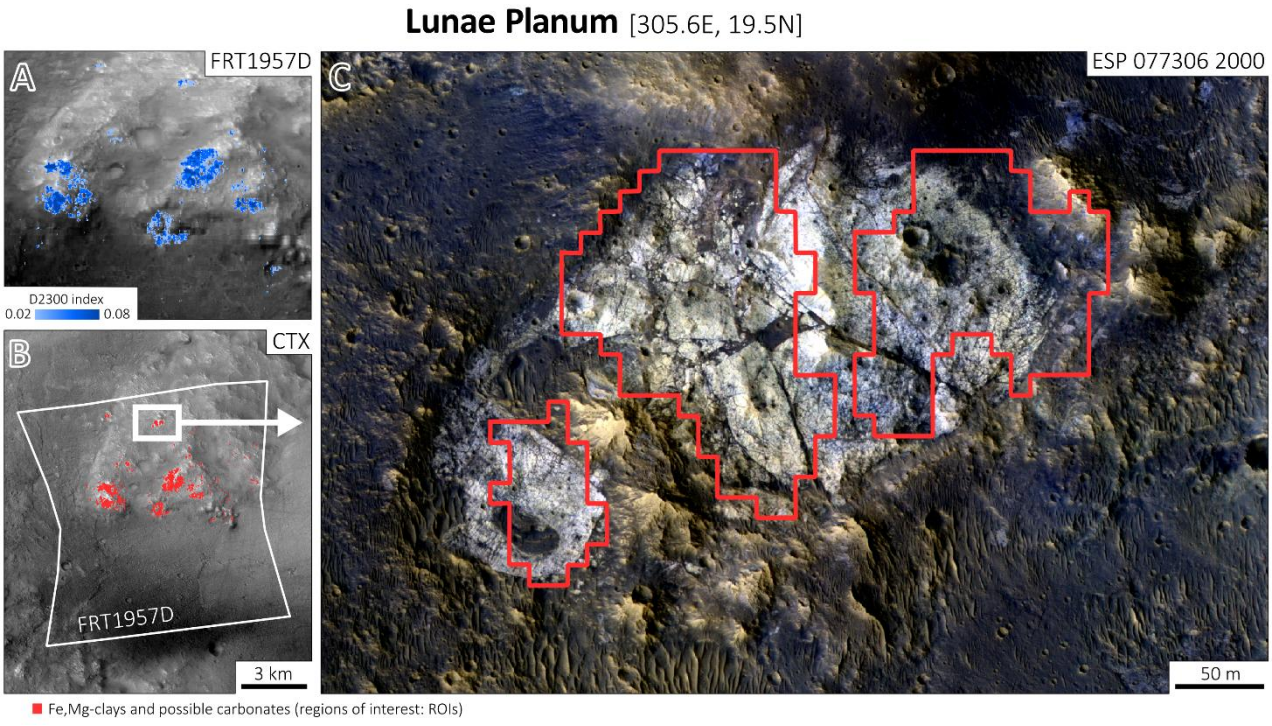


Figure 7 – Clay-bearing outcrops with potential carbonates identified in northeastern Lunae Planum (CRISM FRT1957D cube). (A) Index map showing the spectral parameter "D2300", which highlights a narrow absorption band near 2.3 µm, consistent with ferromagnesian clays and possibly carbonates. Regions of interest (ROIs) are automatically extracted from pixels displaying strong, paired absorptions at 1.9 and 2.3 µm ("BD1900R2" and "D2300", respectively), and are overlaid on the 1.3 µm reflectance ("R1330") to correlate with surface albedo and morphology (37,38). (B) Regional context at CTX scale (6 m·px^{-1}), where the outcrops are mapped in red. (C) HiRISE close-up (25–50 cm·px^{-1}) of representative outcrops identified in FRT1957D (red contours), which commonly occur as fractured, light-toned layers.

Mean CRISM spectra were extracted from each ROI within every cube and examined in detail. Several ROIs display a broad, recurrent absorption near 2.5 µm accompanied by a narrower band at 2.3 µm, consistent with a possible co-occurrence of carbonates. The 2.5 µm band systematically appears in conjunction with the 2.3 µm band, in agreement with previous observations from Nili Fossae, Libya Montes, and Oxia Planum (3,6,25). Beyond 3 µm, carbonates typically show distinct absorptions at 3.4–3.5 µm and around 3.9 µm.

Accurate determination of the positions of diagnostic absorption features is essential for confirming and characterizing carbonate phases. To this end, we derived band centers at 2.3, 2.5 and 3.5 µm by applying continuum removal to each ROI spectrum over the 2.2–2.6 µm (2.3 and 2.5 µm bands) and 3.2–3.6 µm (3.5 µm band) ranges. The continuum represents the spectral baseline and may influence both the apparent position and depth of absorption features within these wavelength ranges (28,46). All band centers and depths extracted in this work are reported in the Supporting Information (**Table S1**).

Spectral mixing behavior of clay-carbonate assemblages

Martian carbonates are systematically mixed with other minerals, particularly clays, at the spatial scale of CRISM observations (18–36 $m \cdot px^{-1}$), thereby complicating their detection. Consequently, spectra from these deposits often exhibit composite or overlapping absorption features arising from multiple mineral components (3,6,20). Moreover, interpretation of spectral slopes in the near-infrared range is further hindered by the presence of ferrous (Fe^{2+}-bearing) phases. A broad absorption near 1 µm, coupled with a steepening of the spectral slope between around 1.1 and 1.8 µm (the "ferrous slope"), can originate from a variety of minerals, including olivine, Fe-rich carbonates, and some clays (20). Consequently, this spectral behavior is not uniquely diagnostic of any single mineral group.

Grain size effects introduce another source of variability, particularly at wavelengths greater than 3 µm (28). Coarser grains tend to produce broader and flatter absorption bands, whereas finer particles yield narrower, more structured features. Although these effects can significantly alter band shapes, they are not explicitly addressed in this study.

While spectral mixing models do not perfectly replicate CRISM observations, they offer valuable guidance for subsequent laboratory analyses. Experimental studies could help reproduce the spectral signatures observed at Oxia Planum (107) and those identified in samples from Jezero and Gale craters (108) by synthesizing mixtures of clays, carbonates, and other relevant phases (e.g., sulfates, olivines). Such efforts would benefit from the use of more representative natural or synthesized compositions, including Fe–Mg carbonates rather than pure endmembers (magnesite, siderite), and intermediate clay minerals such as vermiculites or ferrosaponites, which are likely more widely distributed on Mars (1,2).

To further investigate these effects, we produced a suite of spectral mixing models using the ref. (109) approach, combining an Fe–Mg carbonate (magnesiosiderite) (28) with a ferrosaponite (110). These binary mixtures exhibit several characteristic trends (**Figure 8**), including the disappearance of the 1.4 µm absorption band, likely associated with the emergence of a ferrous slope. Additional weak absorption features

497 near 3.4–3.5 μm are observed in the ferrosaponite sample and may reflect organic contamination. Natural
498 clay samples are known to contain traces of organic compounds that produce C-H stretching absorptions (–
499 CH_2, $–CH_3$) within this spectral range (111,112).

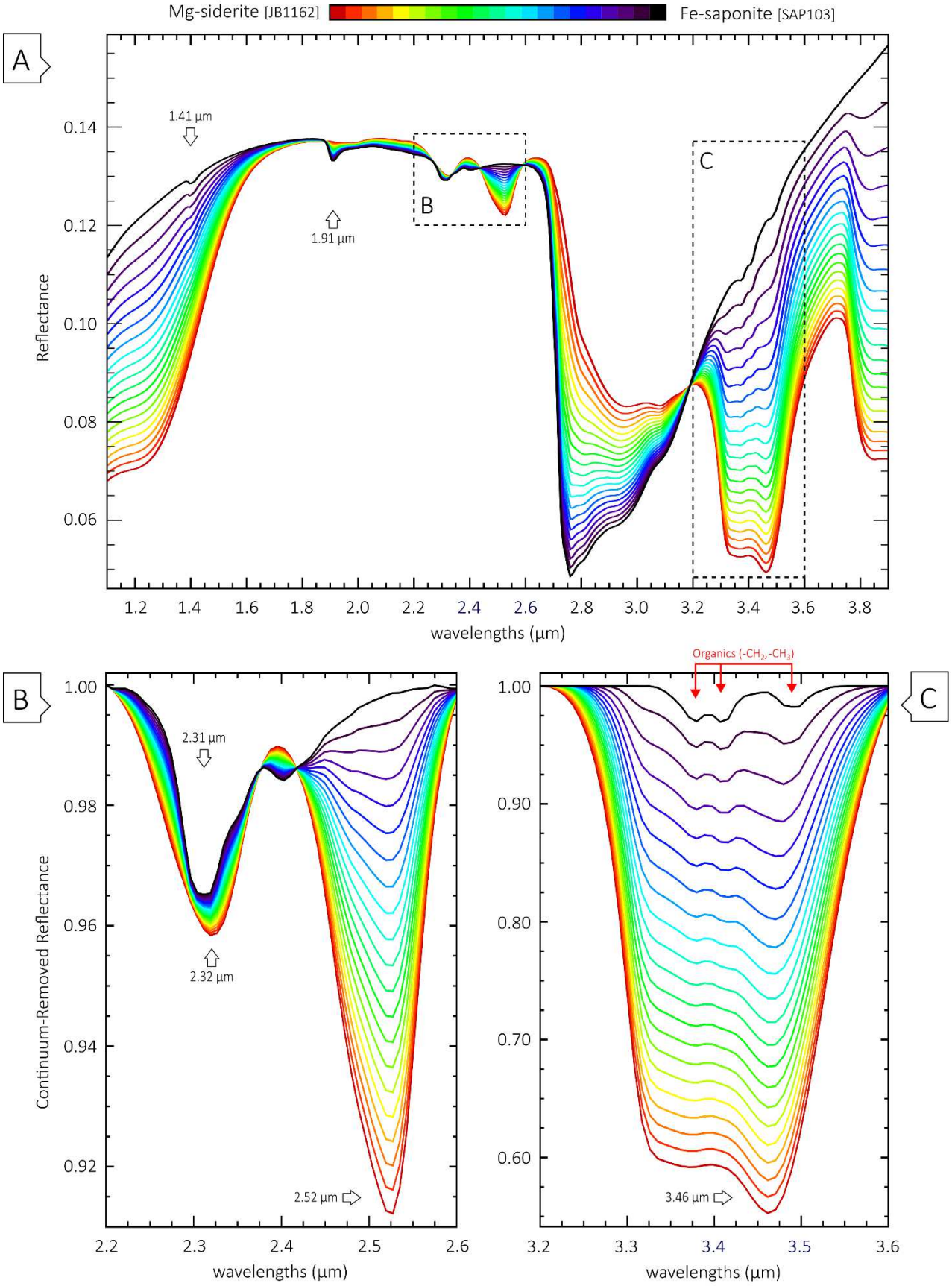


Figure 8 – Spectral mixing modeling using different endmembers: ferrosaponite (SAP103) and magnesiosiderite (JB1162) every 5 wt%. (A) Simulated reflectance (1–4 µm) following ref. (110)'s model to evaluate all major absorption bands near 1.4, 1.9, 2.3, and 2.5 µm, as well as 3.4–3.5 and 3.8–3.9 µm. (B)

Continuum-removed reflectance (2.2–2.6 µm) to emphasize the two absorptions near 2.3 and 2.5 µm. Ferrosaponite does not exhibit absorption near 2.5 µm, which appear purely due to the carbonate. (C) Continuum-removed reflectance (3.2–3.6 µm) to enhance the wide absorption near 3.4–3.5 µm. Band position stands still near 3.46 µm while the absorption deepens with increasing magnesiosiderite content. Multiple subtle bands are also present near 3.38, 3.42 and 3.49 µm associated with organic contamination.

These modeled mixtures indicate that the 2.3 µm absorption remains largely stable with increasing carbonate content, showing only minor shifts in position (**Figure 8**). This band is primarily controlled by the clay component, in agreement with previous findings (20). In contrast, the weaker 2.4 µm absorption, typically associated with ferromagnesian smectites (here ferrosaponite), progressively diminishes and ultimately disappears as carbonate abundance increases. Conversely, the absorptions at 2.5 µm and near 3.5 µm deepen substantially with increasing carbonate content.

Paired absorptions near 2.3 and 2.5 µm are widely reported in carbonate-bearing terrains, particularly in Nili Fossae and Jezero Crater (3,4). However, their distinction from clays and other phyllosilicates primarily resides in the 3–4 µm region (7,23,32). Spectral mixing results further emphasize the diagnostic value of wavelengths beyond 3 µm. Band center positions at 3.5 µm and near 3.9 µm remain largely unaffected by clay contributions and therefore serve as robust indicators of carbonate presence.

These findings highlight the need for a next-generation imaging spectrometer to succeed the now-retired CRISM instrument (2006–2022), whose operations ended after a cryocooler failure. A future instrument would not only enhance carbonate detection but also expand spatial coverage by filling current gaps within and between previously observed regions. It would also enable systematic use of spectral parameters in the 3–4 µm range (3,23,25).

REFERENCES

1. Carter, J., Riu, L., Poulet, F., Bibring, J.-P., Langevin, Y., & Gondet, B. (2023). A Mars orbital catalog of aqueous alteration signatures (MOCAAS). Icarus 389, 115164. https://doi.org/10.1016/j.icarus.2022.115164

2. Brossier, J., Altieri, F., De Sanctis, M.C., Frigeri, A., Ferrari, M., De Angelis, S., Bruschini, E., Rasmussen, M., & Trišić Ponce, J. (2026). Ferromagnesian Clay Diversity across Mars' Crustal Dichotomy: A Window into Early Aqueous Environments. JGR Planets 131, e2025JE009393. https://doi.org/10.1029/2025JE009393

3. Ehlmann, B.L., Mustard, J.F., Murchie, S.L., Poulet, F., Bishop, J.L., Brown, A.J., Calvin, W.M., Clark, R.N., Des Marais, D.J., Milliken, R.E., Roach, L.H., Roush, T.L., Swayze, G.A., & Wray, J.J. (2008). Orbital identification of carbonate-bearing rocks on Mars. Science 322, 1828–1832. https://doi.org/10.1126/science.1164759

4. Brown, A.J., Hook, S.J., Baldridge, A.M., Crowley, J.K., Bridges, N.T., Thomson, B.J., Marion, G.M., de Souza Filho, C.R., & Bishop, J.L. (2010). Hydrothermal formation of clay-carbonate alteration assemblages in the Nili Fossae region of Mars. EPSL 297(1-2), 174–182. https://doi.org/10.1016/j.epsl.2010.06.018

5. Michalski, J.R., & Niles, P.B. (2010). Deep crustal carbonate rocks exposed by meteor impact on Mars. Nature Geosciences 3, 751–755. https://doi.org/10.1038/ngeo971

6. Bishop, J.L., Tirsch, D., Tornabene, L.L., Jaumann, R., McEwen, A.S., McGuire, P.C., Ody, A., Poulet, F., Clark, R.N., Parente, M., McKeown, N.K., Mustard, J.F., Murchie, S.L., Voigt, J., Aydin, Z., Bamberg, M., Petau, A., Michael, G., Seelos, F.P., Hash, C.H., Swayze, G.A., & Neukum, G. (2013). Mineralogy and morphology of geologic units at Libya Montes, Mars: Ancient aqueously derived outcrops, mafic flows, fluvial features, and impacts. JGR Planets 118, 487–513. http://doi.org/10.1029/2012JE004151

7. Wray, J.J., Murchie, S.L., Bishop, J.L., Ehlmann, B.L., Milliken, R.E., Wilhelm, M.B., Seelos, K.D., & Chojnacki, M. (2016). Orbital evidence for more widespread carbonate-bearing rocks on Mars. JGR Planets 121, 652–677. http://dx.doi.org/10.1002/2015JE004972

8. Morris, R.V., Ruff, S.W., Gellert, R., Ming, D.W., Arvidson, R.E., Clark, B.C., Golden, D.C., Siebach, K., Klingelhöfer, G., Schröder, C., Fleischer, I., Yen, A.S., & Squyres, S.W. (2010). Identification of Carbonate-Rich Outcrops on Mars by the Spirit Rover. Science 329, 421–424. https://doi.org/10.1126/science.1189667

9. Clavé, E., Benzerara, K., Meslin, P.-Y., Forni, O., Royer, C., Mandon, L., Beck, P., Quantin-Nataf, C., Beyssac, O., Cousin, A., Bousquet, B., Wiens, R.C., Maurice, S., Dehouck, E., Schroder, S., Gasnault, O., Mangold, N., Dromart, G., Bosak, T., Bernard, S., Udry, A., Anderson, R.B., Arana, G., Brown, A.J., Castro, K., Clegg, S.M., Cloutis, E., Fairen, A.G., Flannery, D.T., Gasda, P.J., Johnson, J.R., Lasue, J., Lopez-Reyes, G., Madariaga, J.M., Manrique, J.A., Le Mouélic, S., Núñez, J.I., Ollila, A.M., Pilleri, P., Pilorget, C., Pinet, P., Poulet, F., Veneranda, M., Wolf, Z.U., & the SuperCam team (2023). Carbonate detection with SuperCam

in igneous rocks on the floor of Jezero Crater, Mars. JGR Planets 128, e2022JE007463. https://doi.org/10.1029/2022JE007463

10. Tutolo, B.M., Hausrath, E.M., Kite, E.S., Rampe, E.B., Bristow, T.F., Downs, R.T., Treiman, A., Peretyazhko, T.S., Thorpe, M.T., Grotzinger, J.P., Roberts, A.L., Archer, P.D., Des Marais, D.J., Blake, D.F., Vaniman, D.T., Morrison, S.M., Chipera, S., Hazen, R.M., Morris, R.V., Tu, V.M., Simpson, S.L., Pandey, A., Yen, A., Larter, S.R., Craig, P., Castle, N., Ming, D.W., Meusburger, J.M., Fraeman, A.A., Burtt, D.G., Franz, H.B., Sutter, B., Clark, J.V., Rapin, W., Bridges, J.C., Loche, M., Gasda, P., Frydenvang, J., & Vasavada, A.R. (2025). Carbonates identified by the Curiosity rover indicate a carbon cycle operated on ancient Mars. Science 388, 292–297. https://dx.doi.org/10.1126/science.ado9966

11. Boynton, W.V., Ming, D.W., Kounaves, S.P., Young, S.M.M., Arvidson, R.E., Hecht, M.H., Hoffma, J., Niles, P.B., Hamara, D.K., Quinn, R.C., Smith, P.H., Sutter, B., Catling, D.C., & Morris, R.V. (2009). Evidence for calcium carbonate at the Mars phoenix landing site. Science 325, 61–64. https://doi.org/10.1126/science.1172768

12. Bandfield, J.L., Glotch, T.D., & Christensen, P.R. (2003). Spectroscopic identification of carbonate minerals in the Martian dust. Science 301, 1084–1087. https://doi.org/10.1126/science.1088054

13. Harvey, R.P., & McSween Jr, H.Y. (1996). A possible high-temperature origin for the carbonates in the Martian meteorite ALH84001. Nature 382, 49–51. https://doi.org/10.1038/382049a0

14. Changela, H.G., & Bridges, J.C. (2011). Alteration assemblages in the nakhlites: Variation with depth on Mars. Meteoritics & Planetary Science 45, 1847–1867. https://doi.org/10.1111/j.1945-5100.2010.01123.x

15. Bridges, J.C., Hicks, L.J., & Treiman, A.H. (2019). Chapter 5: Carbonates on Mars. Volatiles in the Martian crust, 89–118. https://doi.org/10.1016/B978-0-12-804191-8.00005-2

16. Pollack, J.B., Kasting, J.F., Richardson, S.M., & Poliakoff, K. (1987). The case for a warm, wet climate on early Mars. Icarus,71, 203–224. https://doi.org/10.1016/0019-1035(87)90147-3

17. Pollack, J.B., Roush, T., Witteborn, F., Bregman, J., Wooden, D., Stoker, C., Toon, O.B., Rank, D., Dalton, B., & Freedman, R. (1990). Thermal Emission Spectra of Mars (5.4–10.5 μm): Evidence for sulfates, carbonates, and hydrates. JGR Solid Earth 95 (B9), 14,595–14,627. https://doi.org/10.1029/JB095iB09p14595

18. Fairén, A.G., Fernández-Remolar, D., Dohm, J.M., Baker, V.R., & Amils, R. (2004). Inhibition of carbonate synthesis in acidic oceans on early Mars. Nature 431, 423–426. https://doi.org/10.1038/nature02911

19. Bullock, M.A., & Moore, J.M. (2007). Atmospheric conditions on early Mars and the missing layered carbonates. GRL 34, L19201. https://doi.org/10.1029/2007GL030688

20. Bishop, J.L., Perry, K.A., Dyar, M.D., Bristow, T.F., Blake, D.F., Brown, A.J., & Peel, S.E. (2013). Coordinated spectral and XRD analyses of magnesite-nontronite-forsterite mixtures and implications for carbonates on Mars. JGR Planets 118, 635–650. https://doi.org/10.1002/jgre.20066

21. Stack, K.M., & Milliken, R.E. (2015). Modeling near-infrared reflectance spectra of clay and sulfate mixtures and implications for Mars. Icarus 250, 332–356. http://dx.doi.org/10.1016/j.icarus.2014.12.009

22. Sheppard, R.Y., Milliken, R.E., & Robertson, K.M. (2022). Presence of clay minerals can obscure spectral evidence of Mg sulfates: Implications for orbital observations of Mars. Icarus 383, 115083. https://doi.org/10.1016/j.icarus.2022.115083

23. Bultel, B., Viennet, J.-C., Poulet, F., Carter, J., & Werner, S.C. (2019). Detection of Carbonates in Martian Weathering Profiles. JGR Planets 124, 989–1007. http://dx.doi.org/10.1029/2018JE005845

24. Mandon, L., Parkes-Bowen, A., Quantin-Nataf, C., Bridges, J.C., Carter, J., Pan, L., Beck, P., Dehouck, E., Volat, M., Thomas, N., Cremonese, G., Tornabene, L.L., & Thollot, P. (2021). Morphological and spectral diversity of the clay-bearing unit at the ExoMars landing site Oxia Planum. Astrobiology 21, 464–480. https://doi.org/10.1089/ast.2020.2292

25. Brossier, J., Altieri, F., De Sanctis, M.C., Frigeri, A., Ferrari, M., De Angelis, S., Apuzzo, A., Costa, N., & the Ma_MISS team (2022). Constraining the spectral behavior of the clay-bearing outcrops in Oxia Planum, the landing site for ExoMars "Rosalind Franklin" rover. Icarus 386, 115114. https://doi.org/10.1016/j.icarus.2022.115114

26. Scheller, E.L., Swindle, C., Grotzinger, J., Barnhart, H., Bhattacharjee, S., Ehlmann, B., Farley, K., Fischer, W.W., Greenberger, R., Ingalls, M., Martin, P.E., Osorio-Rodriguez, D., & Smith, B.P. (2021). Formation of Magnesium Carbonates on Earth and Implications for Mars. JGR Planets 126, e2021JE006828. https://doi.org/10.1029/2021JE006828

27. Scheller, E.L., Tice, M., Bosak, T., Wordsworth, R., Hurowitz, J., & Weiss, B.P. (2026). Large carbonate reservoir in Mars' crust. Research Square (preprint). https://doi.org/10.21203/rs.3.rs-8264602/v1

28. Bishop, J.L., King, S.J., Lane, M.D., Brown, A.J., Lafuente, B., Hiroi, T., Roberts, R., Swayze, G.A., Lin, J.-F., & Sánchez Román, M. (2021). Spectral properties of anhydrous carbonates and nitrates. Earth and Space Science 8, e2021EA001844. https://doi.org/10.1029/2021EA001844

29. Sutter, B., Dalton, J.B., Ewing, S.A., Amundson, R., & McKay, C.P. (2007). Terrestrial analogs for interpretation of infrared spectra from the Martian surface and subsurface: Sulfate, nitrate, carbonate, and phyllosilicate-bearing Atacama Desert soils. JGR Planets 112. https://doi.org/10.1029/2006JG000313

30. Royer, C., Fouchet, T., Mandon, L., Montmessin, F., Poulet, F., Forni, O., Johnson, J.R., Legett, C., LE Mouélic, S., Gasnault, O., Quantin-Nataf, C., Beck, P., Dehouck, E., Clave, E., Ollila, A.M., Pilorget, C., Bernardi, P., Reess, J.-M., Pilleri, P., Brown, A.J., Newell, R.T., Cloutis, E., Maurice, S., Wiens, R.C., & the

623 SuperCam team (2022). Reflectance of Jezero crater floor: 1. Data processing and calibration of the infrared
624 spectrometer (IRS) on SuperCam. JGR Planets 128, e2022JE007481. https://doi.org/10.1029/2022JE007481

625 31. Sheppard, R.Y., Loizeau, D., Fraeman, A., Rampe, E.B., Pilorget, C., & Bibring, J.-P. (2025). Mg-sulfate
626 can spectrally obscure siderite: Implications for Martian surface carbonates. Frontiers in Astronomical Space
627 Sciences 12, 1549242. https://doi.org/10.3389/fspas.2025.1549242

628 32. Harner, P.L., & Gilmore, M.S. (2015). Visible–near infrared spectra of hydrous carbonates, with
629 implications for the detection of carbonates in hyperspectral data of Mars. Icarus 250, 204–214.
630 http://dx.doi.org/10.1016/j.icarus.2014.11.037

631 33. Leask, E.K., Ehlmann, B.L., Dundar, M.M., Murchie, S.L., & Seelos, F.P. (2018). Challenges in the
632 search for perchlorate and other minerals with 2.1-μm absorptions on Mars. GRL 45, 12,180–12,189.
633 https://doi.org/10.1029/2018GL080077

634 34. Itoh, Y., & Parente, M. (2021). A new method for atmospheric correction and denoising of CRISM
635 hyperspectral data. Icarus 354, 114024. https://doi.org/10.1016/j.icarus.2020.114024

636 35. Murchie, S.L., Arvidson, R., Bedini, P., Beisser, K., Bibring, J.-P., Bishop, J., Boldt, J., Cavender, P.,
637 Choo, T., Clancy, R.T., Darlington, E.H., Des Marais, D., Espiritu, R., Fort, D., Green, R., Guinness, E.,
638 Hayes, J., Hash, C., Heffernan, K., Hemmler, J., Heyler, G., Humm, D., Hutcheson, J., Izenberg, N., Lee, R.,
639 Lees, J., Lohr, D., Malaret, E., Martin, T., McGovern, J.A., McGuire, P., Morris, R., Mustard, J., Pelkey, S.,
640 Rhodes, E., Robinson, M., Roush, T., Schaefer, E., Seagrave, G., Seelos, F., Silverglate, P., Slavney, S.,
641 Smith, M., Shyong, W.-J., Strohbhen, K., Taylor, H., Thompson, P., Tossman, B., Wirzburger, M., & Wolff,
642 M. (2007). Compact Reconnaissance Imaging Spectrometer for Mars (CRISM) on Mars Reconnaissance
643 Orbiter (MRO). JGR Planets 112, E05S03. https://doi.org/10.1029/2006JE002682

644 36. Bishop, J.L., Michalski, J.R., & Carter, J. (2017). Remote Detection of Clay Minerals. Developments in
645 Clay Science 8, 482–514. https://doi.org/10.1016/b978-0-08-100355-8.00014-x

646 37. Pelkey, S.M., Mustard, J.F., Murchie, S.L., Clancy, R.T., Wolff, M., Smith, M., Milliken, R., Bibring, J.-
647 P., Gendrin, A., Poulet, F., Langevin, Y., & Gondet, B. (2007). CRISM multispectral summary products:
648 Parameterizing mineral diversity on Mars from reflectance. JGR Planets 112, E08S14.
649 https://doi.org/10.1029/2006JE002831

650 38. Viviano-Beck, C.E., Seelos, F.P., Murchie, S.L., Kahn, E.G., Seelos, K.D., Taylor, H.W., Taylor, K.,
651 Ehlmann, B.L., Wiseman, S.M., Mustard, J.F., & Morgan, M.F. (2014). Revised CRISM spectral parameters
652 and summary products based on the currently detected mineral diversity on Mars. JGR Planets 119, 1403–
653 1431. https://doi.org/10.1002/2014JE004627

654 39. Brossier, J., Altieri, F., De Sanctis, M.C., Frigeri, A., Ferrari, M., De Angelis, S., Apuzzo, A., & the
655 Ma_MISS team (2023). Spectral Analysis of Clay-bearing Outcrops in Northern Xanthe Terra, Mars:

Comparison with Oxia Planum, the Landing Site for the ExoMars Rover Mission. PSJ 4:27. https://doi.org/10.3847/PSJ/acb3bc

40. Leask, E.K., Ehlmann, B.L., Greenberger, R.N., Pinet, P., Daydou, Y., Ceuleneer, G., & Kelemen, P. (2021). Tracing carbonate formation, serpentinization, and biological materials with micro-/meso-scale infrared imaging spectroscopy in a Mars analogue system, Samail Ophiolite, Oman. Earth and Space Science 8, e2021EA001637. https://doi.org/10.1029/2021EA001637

41. Blaney, D.L., & McCord, T.B. (1989). An observational search for carbonates on Mars. JGR Solid Earth 94 (B8), 10,159–10,166. https://doi.org/10.1029/JB094iB08p10159

42. Wagner, C., & Schade, U. (1996). Measurements and calculations for estimating the spectrometric detection limit for carbonates in Martian soil. Icarus 123 (2), 256–268. https://doi.org/10.1006/icar.1996.0156

43. Murchie, S.L., Seelos, F.P., Hash, C.D., Humm, D.C., Malaret, E., McGovern, J.A., Choo, T.H., Seelos, D.S., Buczkowski, D.L., Morgan, M.F., Barnouin-Jha, O.S., Nair, H., Taylor, H.W., Patterson, G.W., Harvel, C.A., Mustard, J.F., Arvidson, R.E., McGuire, P., Smith, M.D., Wolff, M.J., Titus, T.N., Bibring, J.-P., & Poulet, F. (2009). Compact Reconnaissance Imaging Spectrometer for Mars investigation and data set from the Mars Reconnaissance Orbiter's primary science phase. JGR Planets 114, E00D07. https://doi.org/10.1029/2009JE003344

44. Hunt, G.R., & Salisbury, J.W. (1971). Visible and near infrared spectra of minerals and rocks. II. Carbonates. Modern Geology 2, 23–30. http://refhub.elsevier.com/S0019-1035(14)00678-2/h0320

45. Hunt, G.R. (1977). Spectral signatures of particulate minerals in the visible and near infrared. Geophysics 42 (3), 501–513. https://doi.org/10.1190/1.1440721

46. Bishop, J.L., Lane, M.D., Dyar, M.D., & Brown, A.J. (2008). Reflectance and emission spectroscopy study of four groups of phyllosilicates: Smectites, kaolinite-serpentines, chlorites and micas. Clay Minerals 43, 35–54. https://doi.org/10.1180/claymin.2008.043.1.03

47. Bultel, P., Quantin, C., & Lozach, L. (2015). Description of CoTCAT (Complement to CRISM Analysis Toolkit). IEEE Journal of Selected Topics in Applied Earth Observations and Remote Sensing 8, 3039–3049. https://doi.org/10.1109/JSTARS.2015.2405095

48. Morris, R.V., Haney, N.H., Jakubek, R.S., Fries, M.D., Clark, J.V., Le, L., & Mertzman, S.A. (2022). Relative detectability of iron-bearing phases for the Mars 2020 Sherlock Deep UV Raman instrument: 1. Focusing on carbonates. 53rd LPSC Abstracts, March 7–11, The Woodlands TX, USA, p. 1466. https://www.hou.usra.edu/meetings/lpsc2022/pdf/1466.pdf

49. van Berk, W., Fu, Y., & Ilger, J.-M. (2012). Reproducing early Martian atmospheric carbon dioxide partial pressure by modeling the formation of Mg-Fe-Ca carbonate identified in the Comanche rock outcrops on Mars. JGR Planets 117, E10008. https://doi.org/10.1029/2012JE004173

50. Niles, P.B., Catling, D.C., Berger, G., Chassefière, E., Ehlmann, B.L., Michalski, J.R., Morris, R., Ruff, S.W., & Sutter, B. (2013). Geochemistry of carbonates on Mars: Implications for climate history and nature of aqueous environments. SSR 174, 301–328. https://doi.org/10.1007/s11214-012-9940-y

51. Gil-Lozano, C., Baron, F., Gaudin, A., Lorand, J.-P., Fernandez, V., Hamon, J., & Mangold, N. (2024). The key role of bedrock composition in the formation of carbonates on Mars. Geochemical Perspectives Letters 28, 54–59. https://doi.org/10.7185/geochemlet.2403

52. Beck, P., Beyssac, O., Schmitt, B., Royer, C., Mandon, L., Boulard, E., Rividi, N., & Cloutis, E.A. (2024). Quantification of Crystal Chemistry of Fe-Mg Carbonates by Raman Microspectroscopy and Near-Infrared Remote Sensing. Earth and Space Science 11(9), e2024EA003666. https://doi.org/10.1029/2024EA003666

53. Lin, J.-F., Liu, J., Jacobs, C., & Prakapenka, V.B. (2012). Vibrational and elastic properties of ferromagnesite across the electronic spin-pairing transition of iron. American Mineralogist, 97(4), 583–591. https://doi.org/10.2138/am.2012.3961

54. Chai, L., & Navrotsky, A. (1996). Synthesis, characterization, and enthalpy of mixing of the (Fe,Mg)CO3 solid solution. Geochimica et Cosmochimica Acta 60, 4377–4383. https://doi.org/10.1016/S0016-7037(96)00261-X

55. Ruff, S.W., Hamilton, V.E., Rogers, A.D., Edwards, C.S., & Horgan, B.H.N. (2022). Olivine and carbonate-rich bedrock in Gusev crater and the Nili Fossae region of Mars may be altered ignimbrite deposits. Icarus 380, 114974. https://doi.org/10.1016/j.icarus.2022.114974

56. Mandon, L., Quantin-Nataf, C., Royer, C., Beck, P., Fouchet, T., Johnson, J. R., Dehouck, E., Le Mouélic, S., Poulet, F., Montmessin, F., Pilorget, C., Gasnault, O., Forni, O., Mayhew, L.E., Beyssac, O., Bertrand, T., Clave, E., Pinet, P., Brown, A.J., Legett, C., Tarnas, J., Cloutis, E.A., Poggiali, G., Fornaro, T., Maurice, S., Wiens, R.C., & the SuperCam team (2022). Reflectance of Jezero crater floor: 2. Mineralogical interpretation. JGR Planets 128 (7), e2022JE007450. https://doi.org/10.1029/2022JE007450

57. Thorpe, M.T., Bristow, T.F., Rampe, E.B., Tosca, N.J., Grotzinger, J.P., Bennett, K.A., Achilles, C.N., Blake, D.F., Chipera, S.J., Downs, G., Downs, R.T., Morrison, S.M., Tu, V., Castle, N., Craig, P., De Marais, D.J., Hazen, R.M., Ming, D.W., Morris, R.V., Treiman, A.H., Vaniman, D.T., Yen, A.S., Vasavada, A.R., Dehouck, E., Bridges, J.C., Berger, J., McAdam, A., Peretyazhko, T., Siebach, K.L., Bryk, A.B., Fox, V.K., & Fedo, C.M. (2022). Mars Science Laboratory CheMin data from the Glen Torridon region and the significance of lake-groundwater interactions in interpreting mineralogy and sedimentary history. JGR Planets 127(11), e2021JE007099. https://doi.org/10.1029/2021JE007099

58. Carter, J., & Poulet, F. (2012). Orbital identification of clays and carbonates in Gusev crater. Icarus, 219(1), 250–253. https://doi.org/10.1016/j.icarus.2012.02.024

723 59. Mittlefehldt, D.W. (1994). ALH84001, a cumulate orthopyroxenite member of the Martian meteorite
724 clan. Meteoritics 29, 214–221. https://doi.org/10.1111/j.1945-5100.1994.tb00673.x

725 60. Deer, W.A., Howie, R.A., & Zussman, J. (1992). An introduction to the rock-forming minerals. 2nd
726 Edition, Longman Scientific & Technical, London, 696 pages.

727 61. Deer, W.A., Howie, R.A., & Zussman, J. (2013). An introduction to the rock-forming minerals. 3rd
728 Edition, Mineralogical Society of Great Britain and Ireland, London, UK, 549 pages.
729 https://doi.org/10.1180/DHZ

730 62. Brown, A.J., Viviano, C.E., & Goudge, T.A. (2020). Olivine-Carbonate mineralogy of the Jezero Crater
731 region. JGR Planets 125 (3), e2019JE006011. https://doi.org/10.1029/2019JE006011

732 63. Pokrovsky, O.S., Golubev, S.V., & Schott, J. (2005). Dissolution kinetics of calcite, dolomite and
733 magnesite at 25 °C and 0 to 50 atm pCO2. Chemical Geology 217(3–4), 239–255.
734 https://doi.org/10.1016/j.chemgeo.2004.12.012

735 64. Fernández-Remolar, D.C., Sánchez-Román, M., & Amils, R. (2010). The Case of the Lacking
736 Carbonates and the Emergence of Early Life on Mars. Sustainability 2, 2541–2554.
737 https://doi.org/10.3390/su2082541

738 65. Davis, N.E., Newman, J., Wheelock, P.B., & Kronenberg, A.K. (2011). Grain Growth Kinetics of
739 Dolomite, Magnesite and Calcite: A Comparative Study, Physics & Chemistry of Minerals 38, 123–138.
740 https://doi.org/10.1007/s00269-010-0389-9

741 66. Santos, H.S., Nguyen, H., Venancio, F., Ramteke, D., Zevenhoven, R., & Kinnunen, P. (2023).
742 Mechanisms of Mg carbonates precipitation and implications for CO2 capture and utilization/storage.
743 Inorganic Chemistry Frontiers 10, 2507. https://doi.org/10.1039/d2qi02482a

744 67. Wordsworth, R.D., Knoll, A.H., Hurowitz, J., Baum, M., Ehlmann, B.L., Head, J.W., & Steakley, K.
745 (2021). A coupled model of episodic warming, oxidation and geochemical transitions on early Mars. Nature
746 Geosciences 14, 127–132. https://doi.org/10.1038/s41561-021-00701-8

747 68. Kite, E.S., & Noblet A. (2022). High and Dry: Billion-Year Trends in the Aridity of River-Forming
748 Climates on Mars. GRL 49, e2022GL101150. https://doi.org/10.1029/2022GL101150

749 69. Kite, E.S., Tutolo, B.M., Turner, M.L., Franz, H.B., Burtt, D.G., Bristow, T.F., Fischer, W.W., Milliken,
750 R.E., Fraeman, A.A., & Zhou, D.Y. (2025). Carbonate formation and fluctuating habitability on Mars. Nature
751 643, 60–66. https://doi.org/10.1038/s41586-025-09161-1

752 70. Berner, R.A. (1975). The role of magnesium in the crystal growth of calcite and aragonite from sea water.
753 Geochimica et Cosmochimica Acta 39, 489–494. https://doi.org/10.1016/0016-7037(75)90102-7

754 71. Davis, K.J., Dove, P.M., & De Yoreo, J.J. (2000). The role of Mg2+ as an impurity in calcite growth.
755 Science 290, 1134–1137. https://doi.org/10.1126/science.290.5494.1134

72. Pan, Y., Li, Y., Ma, Q., He, H., Wang, S., Sun, Z., Cai, W.-J., Dong, B., Di, Y., Fu, W., & Chen, C.-T. A. (2021). The role of Mg2+ in inhibiting CaCO3 precipitation from seawater. Marine Chemistry 237, 104036. https://doi.org/10.1016/j.marchem.2021.104036

73. Zastrow, A.M., & Glotch, T.D. (2021). Distinct carbonate lithologies in Jezero crater, Mars. GRL 48, e2020GL092365. https://doi.org/10.1029/2020GL092365

74. Rividi, N., van Zuilen, M., Philippot, P., Ménez, B., Godard, G., & Poidatz, E. (2010). Calibration of Carbonate Composition Using Micro-Raman Analysis: Application to Planetary Surface Exploration. Astrobiology 10 (3), 293–309. https://doi.org/10.1089/ast.2009.0388

75. Boulard, E., Guyot, F., & Fiquet, G. (2012). The influence on Fe content on Raman spectra and unit cell parameters of magnesite–siderite solid solutions. Physics and Chemistry of Minerals 39, 239–246. https://doi.org/10.1007/s00269-011-0479-3

76. Gaffey, S.J. (1987). Spectral reflectance of carbonate minerals in the visible and near infrared (0.35–2.55 μm): Anhydrous carbonate minerals. JGR Solid Earth 92 (B2), 1429–1440. https://doi.org/10.1029/JB092iB02p01429

77. Torres Auré, I., Carter, J., Quantin-Nataf, C., Loizeau, D., Dehouck, E., & Volat, M. (2026). Clay continuity between Oxia Planum and Mawrth Vallis. Icarus, in press. https://doi.org/10.1016/j.icarus.2026.117113

78. Schwertmann, U. & Murad, E. (1983). Effect of pH on the Formation of Goethite and Hematite from Ferrihydrite. Clays Clay Minerals 31, 277–284. https://doi.org/10.1346/CCMN.1983.0310405

79. Niles, P.B., Zolotov, M.Y., & Leshin, L.A. (2009). Insights into the formation of Fe- and Mg-rich aqueous solutions on early Mars provided by the ALH 84001 carbonates. EPSL 286 (1–2), 122–130. https://doi.org/10.1016/j.epsl.2009.06.039

80. Hausrath, E.M., & Olsen, A.A. (2013). Using the chemical composition of carbonate rocks on Mars as a record of secondary interaction with liquid water. American Mineralogist 98 (5–6), 897–906. https://doi.org/10.2138/am.2013.4187

81. De Sanctis, M.C., Raponi, A., Ammannito, E., Ciarniello, M., Toplis, M.J., McSween, H.Y., Castillo-Rogez, J.C., Ehlmann, B.L., Carrozzo, F.G., Marchi, S., Tosi, F., Zambon, F., Capaccioni, F., Capria, M.T., Fonte, S., Formisano, M., Frigeri, A., Giardino, M., Longobardo, A., Magni, G., Palomba, E., McFadden, L.A., Pieters, C.M., Jaumann, R., Schenk, P., Mugnuolo, R., Raymond, C.A., & Russel, C.T. (2016). Bright carbonate deposits as evidence of aqueous alteration on (1) Ceres. Nature 536, 54–57. https://doi.org/10.1038/nature18290

82. Raponi, A., De Sanctis, M.C., Carrozzo, F.G., Ciarniello, m., Castillo-Rogez, J.C., Ammannito, E., Frigeri, A., Longobardo, A., Palomba, E., Tosi, F., Zambon, F., Raymond, C.A., & Russell, C.T. (2018).

Mineralogy of Occator crater on Ceres and insight into its evolution from the properties of carbonates, phyllosilicates, and chlorides. Icarus 320, 83–96. https://doi.org/10.1016/j.icarus.2018.02.001

83. Fukai, R., Nishimura, M., Yumoto, K., Cho, Y., Shimizu, Y., Matsuoka, M., Tatsumi, E., Furukawa, S., Sakurai, R., Yada, T., Hatakeda, K., Yogata, K., Enokido, Y., Tahara, R., Miyazaki, A., Kawasaki, S., Kanemaru, R., Sugita, S., Mori, S., Nakahara, S., Aikyo, Y., Miyamoto, H., Pilorget, C., Loizeau, D., Nardelli, L., Sheppard, R., Lantz, C., Riu, L., Bibring, J.-P., Brunetto, R., Okada, T., Abe, M., & Usui, T. (2025). Nondestructive analysis of Bennu samples toward comparative studies with Ryugu samples. Meteoritics & Planetary Science 61, 3–16. https://doi.org/10.1111/maps.70077

84. Pilorget, C., Okada, T., Bibring, J.-P., Loizeau, D., Hatakeda, K., Nardelli, L., Riu, L., Sheppard, R., Jiang, T., Mahlke, M., Brunetto, R., Baklouti, D., Fukai, R., Abe, M., Aleon-Toppani, A., Enokido, Y., Hamm, V., Kawasaki, S., Lantz, C., Miyazaki, A., Moussi-Soffys, A., Nishimura, M., Poulet, F., Tahara, R., Usui, T., Yada, T., & Yogata, K. (2025). Bennu and Ryugu constituents from samples IR analyses and potential source of terrestrial planets' ingredients. Nature Communications 16, 9532. https://doi.org/10.1038/s41467-025-65438-z

85. Lee, M.R., Lindgren, P., & Sofe, M.R. (2014). Aragonite, breunnerite, calcite and dolomite in the CM carbonaceous chondrites: High fidelity recorders of progressive parent body aqueous alteration. Geochimica et Cosmochimica Acta 144, 126–156. https://doi.org/10.1016/j.gca.2014.08.019

86. Lindgren, P., Lee, M.R., Starkey, N.A., & Franchi, I.A. (2017). Fluid evolution in CM carbonaceous chondrites tracked through the oxygen isotopic compositions of carbonates. Geochimica et Cosmochimica Acta 204, 240–251. https://doi.org/10.1016/j.gca.2017.01.048

87. King, A.J., Schofield, P.F., & Russell, S.S. (2017). Type 1 aqueous alteration in CM carbonaceous chondrites: Implications for the evolution of water-rich asteroids. Meteoritics & Planetary Science 52(6), 1197–1215. https://doi.org/10.1111/maps.12872

88. Bristow, T.F., Kennedy, M.J., Morrison, K.D., & Mrofka, D.D. (2012). The influence of authigenic clay formation on the mineralogy and stable isotopic record of lacustrine carbonates. Geochimica et Cosmochimica Acta 90, 64–82. http://dx.doi.org/10.1016/j.gca.2012.05.006

89. Cupertino, D.F., Ramnani, C.W., Vanden Berg, M.D., & Awramik, S.M. (2023). Formation of magnesium-clay in a lacustrine microbialite-bearing carbonate deposit, Eocene Green River Formation, Sanpete County, Utah. Sedimentology 71, 263–292. https://doi.org/10.1111/sed.13136

90. Brown, A.J., Walter, M.R., & Cudahy, T.J. (2005). Hyperspectral Imaging Spectroscopy of a Mars Analog Environment at the North Pole Dome, Pilbara Craton, Western Australia. Australian Journal of Earth Sciences 52, 353–364. https://doi.org/10.1080/08120090500134530

821 91. Diaz, N., King, G.E., Valla, P.G., Herman, F., & Verrecchia, E.P. (2016). Pedogenic carbonate nodules as
822 soil time archives: Challenges and investigations related to OSL dating. Quaternary Geochronology 36, 120–
823 133. https://doi.org/10.1016/j.quageo.2016.08.008

824 92. Dietrich, F., Diaz, N., Deschamps, P., Ngounou Ngatcha, B., Sebag, D., & Verrecchia, E.P. (2017). Origin
825 of calcium in pedogenic carbonate nodules from silicate watersheds in the Far North Region of Cameroon:
826 Respective contribution of in situ weathering source and dust input. Chemical Geology 460, 54–69.
827 https://doi.org/10.1016/j.chemgeo.2017.04.015

828 93. Bruschini, E., Ferrari, M., Mazzoni, C., Fazi, S., Chiocci, F.L., Mazzini, I., Costanzo, G., De Angelis, S.,
829 De Sanctis, M.C., Altieri, F., Brossier, J., & Ammannito, E. (2024). Preliminary spectroscopic investigation
830 of a potential Mars analog site: Lake Bagno dell'Acqua, Pantelleria, Italy. PSS 245, 105893.
831 https://doi.org/10.1016/j.pss.2024.105893

832 94. Mazzoni, C., Piacentini, A., Di Bella, L., Aldega, L., Perinelli, C., Conte, A.M., Ingrassia, M.,
833 Ruspandini, T., Bonfanti, A., Caraba, B., Falese, F.G., Chiocci, F.L., & Fazi, S. (2024). Carbonate
834 precipitation and phosphate trapping by microbialite isolates from an alkaline insular lake (Bagno
835 dell'Acqua, Pantelleria Island, Italy). Frontiers in Microbiology 15, 1–17.
836 https://doi.org/10.3389/fmicb.2024.1391968

837 95. Viviano, C.E., Moersch, J.E., & McSween, H.Y. (2013). Implications for early hydrothermal
838 environments on Mars through the spectral evidence for carbonation and chloritization reactions in the Nili
839 Fossae region. JGR 118, 1719–1954. https://doi.org/10.1002%2Fjgre.20141

840 96. Ravanis, E., Bedford, C.C., Horgan, B., Garczynski, B., Vaughan, A., Johnson, J.R., Rice, M., Jones, A.J.,
841 Fagents, S., Klidaras, A., Gupta, S., Núñez, J., Lapo, K., Cloutis, E.A., Bell III, J.F., Wiens, R.C., & Brown,
842 A.J. (2026). Formation and Alteration of Olivine-Carbonate Rocks Within Jezero Crater as Constrained by In
843 Situ Visible/Near-Infrared Multispectral Images. JGR Planets 131, e2025JE009151.
844 https://doi.org/10.1029%2F2025JE009151

845 97. [dataset] Brossier, J. (2026). Are Carbonates Hiding Among Mars's Ferromagnesian Clays? – Supporting
846 Datasets. Figshare. https://doi.org/10.6084/m9.figshare.30932855

847 Private link (for review): https://figshare.com/s/06bb982abc9fa0cfcc51

848 ***Data & Methods***

849 98. Bibring, J.-P., Langevin, Y., Mustard, J.F., Poulet, F., Arvidson, R., Gendrin, A., Gondet, B., Mangold, N.,
850 Pinet, P., Forget, F., on behalf of the OMEGA team, Berthé, M., Bibring, J.-P., Gendrin, Gomez, C., Gondet,
851 B., Jouglet, D., Poulet, F., Souflot, A., Vincendon, M., Combes, M., Drossart, P., Encrenaz, T., Fouchet, T.,
852 Merchiorri, R., Belluci, G., Altieri, F., Formisano, V., Capaccioni, F., Cerroni, P., Coradini, A., Fonti, S.,
853 Korablev, O., Kottsov, V., Ignatiev, N., Moroz, V., Titov, D., Zasova, L., Loizeau, D., Mangold, N., Pinet, P.,
854 Douté, S., Schmitt, B., Sotin, C., Hauber, E., Hoffmann, H., Jaumann, R., Keller, U., Arvidson, R., Mustard,

J.F., Duxbury, T., Forget, F., & Neukum, G. (2006). Global mineralogical and aqueous Mars history derived from OMEGA/Mars Express data. Science 312, 400–404. https://doi.org/10.1126/science.1122659

99. Poulet, F., Gomez, C., Bibring, J.-P., Langevin, Y., Gondet, B., Pinet, P., Belluci, G., & Mustard, J.F. (2007). Martian surface mineralogy from Observatoire pour la Minéralogie, l'Eau, les Glaces et l'Activité on board the Mars Express spacecraft (OMEGA/MEx): Global mineral maps. JGR Planets 112, E08S02. https://doi.org/10.1029/2006JE002840

100. Mustard, J.F., Murchie, S.L., Pelkey, S.M., Ehlmann, B.L., Milliken, R.E., Grant, J.A., Bibring, J.-P., Poulet, F., Bishop, J., Noe Dobrea, E., Roach, L., Seelos, F., Arvidson, R.E., Wiseman, S., Green, R., Hash, C., Humm, D., Malaret, E., McGovern, J.A., Seelos, K., Clancy, T., Clark, R., De Marais, D., Izenberg, N., Knudson, A., Langevin, Y., Martin, T., McGuire, P., Morris, R., Robinson, M., Roush, T., Smith, M., Swayze, G., Taylor, H., Titus, T., & Wolff, M. (2008). Hydrated silicate minerals on Mars observed by the Mars Reconnaissance Orbiter CRISM instrument. Nature 454, 305–309. https://doi.org/10.1038/nature07097

101. Swayze, G.A. (2004). Using reflectance spectroscopy to evaluate minerals of environmental concern, in Infrared Spectroscopy in Geochemistry, Exploration Geochemistry, and Remote Sensing, edited by King, P.L., Ramsey, M.S., & Swayze, G.A., Mineralogical Association of Canada, Short Course Series volume 3, 181–196. https://doi.org/10.3749/9780921294771.ch07

102. Cloutis, E.A., Hawthorne, F.C., Mertzman, S.A., Krenn, K., Craig, M.A., Marcino, D., Methot, M., Strong, J., Mustard, J.F., Blaney, D.L., Bell III, J.F., & Vilas, F. (2006). Detection and discrimination of sulfate minerals using reflectance spectroscopy. Icarus 184, 121–157. http://dx.doi.org/10.1016/j.icarus.2006.04.003

103. Parente, M., Clark, J.T., Brown, A.J., & Bishop, J.L. (2010). End-to-end simulation and analytical model of remote sensing systems: Application to CRISM. IEEE Transactions on Geosciences and Remote Sensing 48, 3877–3888. https://doi.org/10.1109/TGRS.2010.2050000

104. Bultel, B., Quantin-Nataf, C., Andréani, M., Clénet, H., & Lozac'h, L. (2015). Deep alteration between Hellas and Isidis Basins. Icarus 260, 141–160. http://dx.doi.org/10.1016/j.icarus.2015.06.037

105. Platt, R., Al Zayer, Z., Arcucci, R., & John, C.M. (2025). Teaching Ourselves to See: A Direct Method for Denoising CRISM Hyperspectral Data. IEEE Transactions on Geoscience and Remote Sensing. https://doi.org/10.1109/TGRS.2025.3591569

106. McGuire, P.C., Bishop, J.L., Brown, A.J., Fraeman, A.A., Marzo, G.A., Morgan, M.F., Murchie, S.L., Mustard, J.F., Parente, M., Pelkey, S.M., Roush, T.L., Seelos, F.P., Smith, M.D., Wendt, L., & Wolff, M.J. (2009). An improvement to the volcano-scan algorithm for atmospheric correction of CRISM and OMEGA spectral data. PSS 57, 809–815. https://doi.org/10.1016/j.pss.2009.03.007

107. Dugdale, A., Ramkissoon, N.K., Fawdon, P., Patel, M.R., Hills, L., Degli-Alessandrini, G., Bonsall, E., Schröder, C., Turner, S.M.R., Achilles, C.N., & Pearson, V.K. (2023). SOPHIA: A mineralogical simulant for

889 phyllosilicate terrains at the Rosalind Franklin landing site, Oxia Planum, Mars. Icarus 400, 115568.
890 https://doi.org/10.1016/j.icarus.2023.115568

891 108. Bruschini, E., Ferrari, M., Pisello, A., Brossier, J., De Sanctis, M.C., & Altieri, F. (2025). Spectroscopic
892 investigation of synthetic Martian analog mineral mixtures relevant to Gale and Jezero Craters Exploration.
893 Earth and Space Science 12, e2025EA004386. https://doi.org/10.1029/2025EA004386

894 109. Hapke, B. (2012). Theory of reflectance and emittance spectroscopy (topics in remote sensing).
895 Cambridge Univ. Press, Cambridge, UK, 2nd edition, pp. 513. https://doi.org/10.1017/CBO9781139025683

896 110. Treiman, A.H., Morris, R.V., Agresti, D.G., Graff, T.G., Achilles, C.N., Rampe, E.B., Bristow, T.F.,
897 Blake, D.F., Vaniman, D.T., Bish, D.L., Chipera, S.J., Morrison, S.M., & Downs, R.T. (2014). Ferrian
898 saponite from the Santa Monica Mountains (California, U.S.A., Earth): Characterization as an analog for
899 clay minerals on Mars with application to Yellowknife Bay in Gale Crater. American Mineralogist 99, 2234–
900 2250. http://dx.doi.org/10.2138/am-2014-4763

901 111. Moroz, L.V., Arnold, G., Korochantsev, A.V., & Waesch, R. (1998). Natural Solid Bitumens as Possible
902 Analogs for Cometary and Asteroid Organics: 1. Reflectance Spectroscopy of Pure Bitumens. Icarus 134(2),
903 253–268. https://doi.org/10.1006/icar.1998.5955

904 112. Orthous-Daunay, F.-R., Quirico, E., Beck, P., Brissaud, O., Dartois, E., Pino, T., & Schmitt, B. (2013).
905 Mid-infrared study of the molecular structure variability of insoluble organic matter from primitive
906 chondrites. Icarus 223, 534–543. https://doi.org/10.1016/j.icarus.2013.01.003

Supplementary Files

This is a list of supplementary files associated with this preprint. Click to download.

- TableS1.xlsx
- TableS2.xlsx
- SupportingMaterials.pdf